Electronic Supplementary Information

AIE-active mechanoluminescent discotic liquid crystals for applications in OLEDs and bio-imaging

Joydip De,[a] Abdul Haseeb M. M.,[a] Rohit Ashok Kumar Yadav,[b] Santosh Prasad Gupta,[c] Indu Bala,[a] Prateek Chawla,[d] Kiran Kishore Kesavan,[b] Jwo-Huei Jou,[b] and Santanu Kumar Pal*[a]

[a]*Department of Chemical Sciences, Indian Institute of Science Education and Research (IISER) Mohali, Knowledge city, Sector 81, SAS Nagar, Manauli 140306, India*
[b]*Department of Materials Science and Engineering, National Tsing Hua University, Hsinchu 30013, Taiwan*
[c]*Department of Physics, Patna University, Patna-800005, India*
[d]*Department of Biological Sciences, Indian Institute of Science Education and Research (IISER) Mohali, Knowledge city, Sector 81, SAS Nagar, Manauli 140306, India*

E-mail: skpal@iisermohali.ac.in, santanupal.20@gmail.com

Table of Contents **Page No.**

1) Materials and methods

Materials: Chemicals and solvents (AR quality) were used as received without any further purification. Column chromatographic separations were performed on silica gel (100-200 & 230-400 mesh). Thin layer chromatography (TLC) was performed on aluminium sheets pre-coated with silica gel (Merck, Kieselgel 60, F254).

Measurements and characterization: *The instrumental details for structural characterization (NMR, HRMS, FT-IR) thermal characterization (polarized optical Microscopy (POM), Thermogravimetric analysis (TGA), Differential scanning calorimetry (DSC), small and wide angle X-ray scattering (SAXS/WAXS), photophysical studies (UV-vis & Fluorescence), electrochemical (Cyclic voltammetry), electroluminescence (OLEDs) characterization are similar to as mentioned in our previous papers and reproduced below for the reader's convenience.*[1]

"Structural characterization of the compounds was carried out through a combination of infrared spectroscopy (IR) (Perkin Elmer Spectrum Two), ^{1}H NMR and ^{13}C NMR (Bruker Biospin Switzerland Avance-iii 400 MHz and 100 MHz spectrometers respectively), UV-vis-NIR spectrophotometers (Agilent Technologies, Cary 5000) and Mass spectrometry (Water Synapt G-2-s QTOF with MALDI ion source and α-cyano-4-hydroxy-cinnamic acid as a matrix). IR spectra were recorded in neat form for target compounds. ^{1}H NMR spectra were recorded using deuterated chloroform ($CDCl_3$) as solvent and tetramethylsilane (TMS) as an internal standard. All the UV-vis experiments were performed in 10^{-6} M $CHCl_3$ solutions. Cyclic Voltammetry (CV) experiments were performed by using Princeton Applied Research VersaSTAT 3. The transition temperatures and associated enthalpy values were determined using a differential scanning calorimeter (Perkin Elmer DSC 8000 coupled to a controlled liquid nitrogen accessory (CLN 2)) which was operated at a scanning rate of 10 °C min^{-1} both on heating and cooling. Thermogravimetric analysis (TGA) was carried out from 25 to 500 °C (at a heating rate of 10 °C min^{-1}) under nitrogen atmosphere on a Shimadzu DTG-60 instrument. Textural observations of the mesophase were performed with Nikon Eclipse LV100POL polarizing optical microscope (POM) provided with a Linkam heating stage (LTS 420). All images were captured using a Q-imaging camera. Small and wide angle X-ray scattering (SAXS/WAXS) experiments were carried out by filling samples in glass capillaries using Cu-K_α (λ = 1.5418 Å) radiation from Xeuss (Model C HP100 fm) X-ray diffractometer from Xenocs equipped with GeniX 3D source operating at 50 kV and 0.6 mA in conjunction with a multilayer mirror and Pilatus 200 hybrid pixel detector from Dectris. For electroluminescence measurements compound **1.1-1.3** used as the dopants and OLED devices were fabricated by a solution-processed approach. In these OLEDs, a layer of 35 nm thick poly(3,4-ethylenedioxythiophene)polystyrene sulfonate (PEDOT:PSS) was spin-coated onto the pre-cleaned and patterned ITO substrate, which was utilized as a hole injection layer. 4,4′-bis(N-carbazolyl)-1,1′-biphenyl (CBP) was used as the host matrix, while 2,2',2"-(1,3,5-Benzinetriyl)-tris(1-phenyl-1-H-benzimidazole) (TPBi) (40 nm layer) served as the electron-transporting layer. LiF and Al were used as the composite cathode. The electroluminescence (EL) spectra were recorded using a spectra scan spectroradiometer, Photo Research PR-655. The features of the current-density and brightness versus applied voltage were simultaneously obtained by combining a Keithley 2400 and PR-655."

Cell culture and cellular imaging details:

HeLa cells (from ATCC) were cultured in DMEM (Lonza) supplemented with 10 % FBS (Gibco) at 37 °C with 5% CO_2, in a humified cell culture chamber. Each line was passaged for no more than 15 passages.

For live-imaging, cells were seeded on a 35 mm glass-bottom cell imaging dish at a density of 1×10^5 cells per dish. The media was changed after 24 hours and fresh media (with the desired concentration of the compound) was added. The dish was incubated at 37 °C, in a humified cell culture chamber, for 3 hours. For co-localization, cells were incubated with 7.5 μM of the compound for 2 hours followed by 100 nM of LysoTracker Red DND-99 (ThermoFisher Scientific, Catalogue No. L7528) for 1 hour. Ezcount™ MTT cell assay kit (HiMedia, Catalogue Number: CCK003) was used for assessing the cytotoxicity of the compound.

Single-plane confocal images were acquired by using a 710 confocal laser scanning microscope (ZEISS) and ZEN Pro 2011 (ZEISS) software was used for image acquisition. Correlation of the fluorescence signal and adjustment to brightness/contrast was performed using *ImageJ* software.

2) Synthesis and characterization details

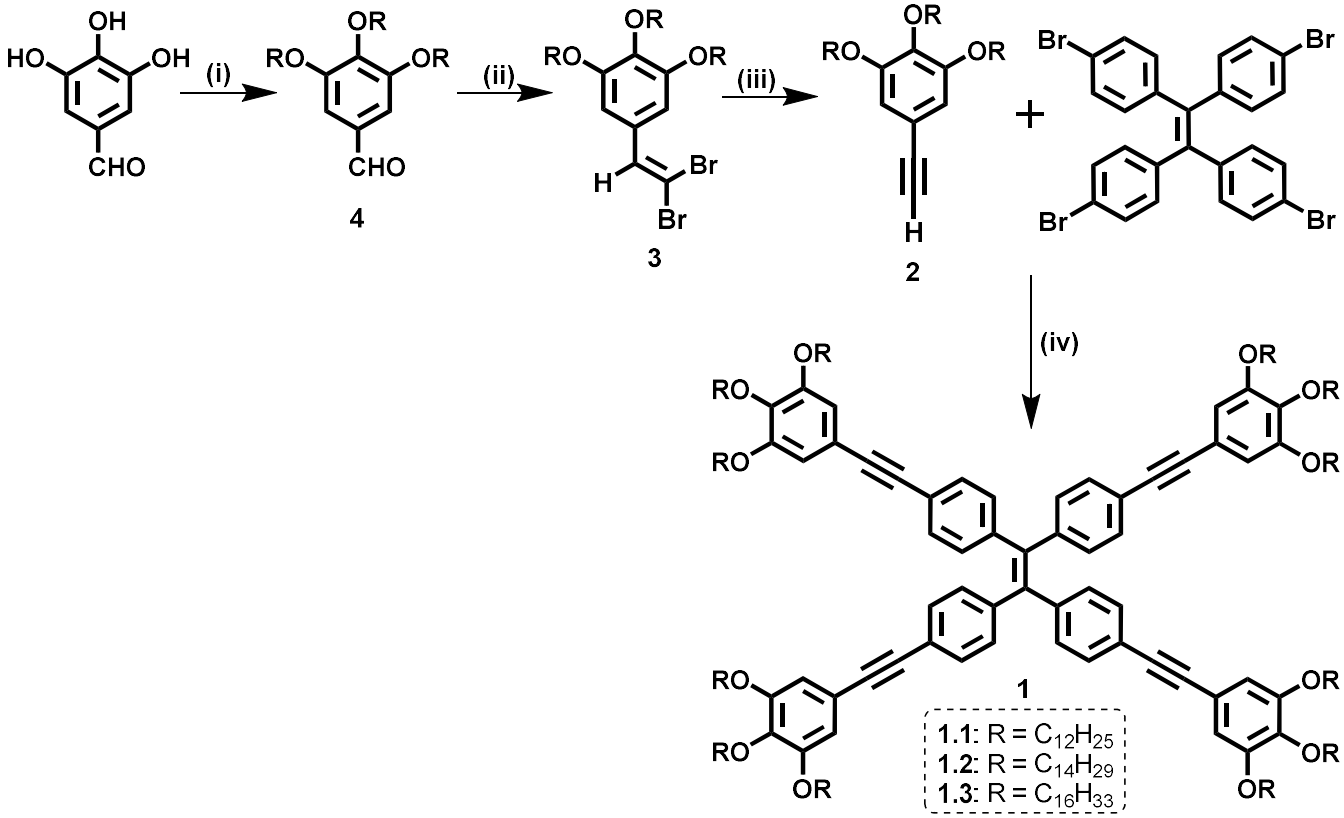

Scheme S1 Synthesis of tetraphenylethene (TPE) derivatives **1**. Reagents: (i) K_2CO_3, RBr, KI, DMF (dry), 90 °C, 18h; (ii) CBr_4, PPh_3, dry DCM, 0.5 h; (iii) n-BuLi, dry-THF, r.t., 48 h; (iv) $Pd(PPh_3)_2Cl_2$, CuI, PPh_3, Et_3N (dry), DMF (dry), 90 °C, 18h. Yield of **1**: 79-84%

Experimental procedure:

Synthesis of 1,1,2,2-tetrakis(4-((3,4,5-tris(dodecyloxy)phenyl)ethynyl)phenyl)ethene (1.1):

In a 100 ml two-neck round bottomed flask dry triethylamine (40 mL) and dry DMF (15 mL) were added and purge it with N_2 gas for 15 minutes. After that $Pd(PPh_3)_2Cl_2$ (37.89 mg, 0.081 equiv), CuI (15.11 mg, 0.119 equiv)**,** PPh_3 (21.33 mg, 0.122 equiv), 1,2,3-tris(dodecyloxy)-5-ethynylbenzene **2**[2] (2.62 g, 6 equiv) and 1,1,2,2-tetrakis(4-bromophenyl)ethene (431.90 mg, 1 equiv) were sequentially added in the solvent mixture and purge it with N_2 gas for 15 minutes. Then the reaction mixture was refluxed at 90 °C for 24 hours. The reaction solution was cooled and the solvent was removed by rotary evaporation. Then, organic layer was extracted by performing the diethyl ether/water extraction. The diethyl ether extracts were dried over anhydrous sodium sulfate. After concentrating, the target material was purified by using column chromatography (neutral alumina, Ethylacetate/Hexane (0.7:99.3)) to get the product as yellow solid (79 % yield).

^{1}H NMR (400 MHz, $CDCl_3$, δ ppm): 7.28 (d, J = 7.8 Hz, 8H), 7.00 (d, J = 7.88 Hz, 8H), 6.70 (s, 8H), 3.96 (t, J = 6.38 Hz, 24H), 1.83-1.72 (m, 24H), 1.48-1.41 (m, 24H), 1.33-1.24 (m, 192H), 0.88 (t, J = 6.48 Hz, 36H).

^{13}C NMR (100 MHz, $CDCl_3$, δ ppm): 153.11, 143.02, 141.02, 139.18, 131.57, 131.23, 121.98, 117.66, 110.15, 90.65, 88.17, 73.67, 69.21, 32.08, 30.46, 29.90, 29.89, 29.85, 29.81, 29.79, 29.75, 29.64, 29.55, 29.52, 29.47, 26.23, 22.85, 14.27.

IR (Neat, KBr, ν_{max}/cm^{-1}): 2955.50, 2923.65, 2853.41, 1573.43, 1508.06, 1467.30, 1419.29, 1379.56, 1354.52, 1258.46, 1234.23, 1117.35, 830.96, 748.74, 721.47.

MALDI-MS: *m/z* calcd for $C_{202}H_{325}O_{12}$ $(M+H)^+$: 2943.4821. Found: 2943.5581.

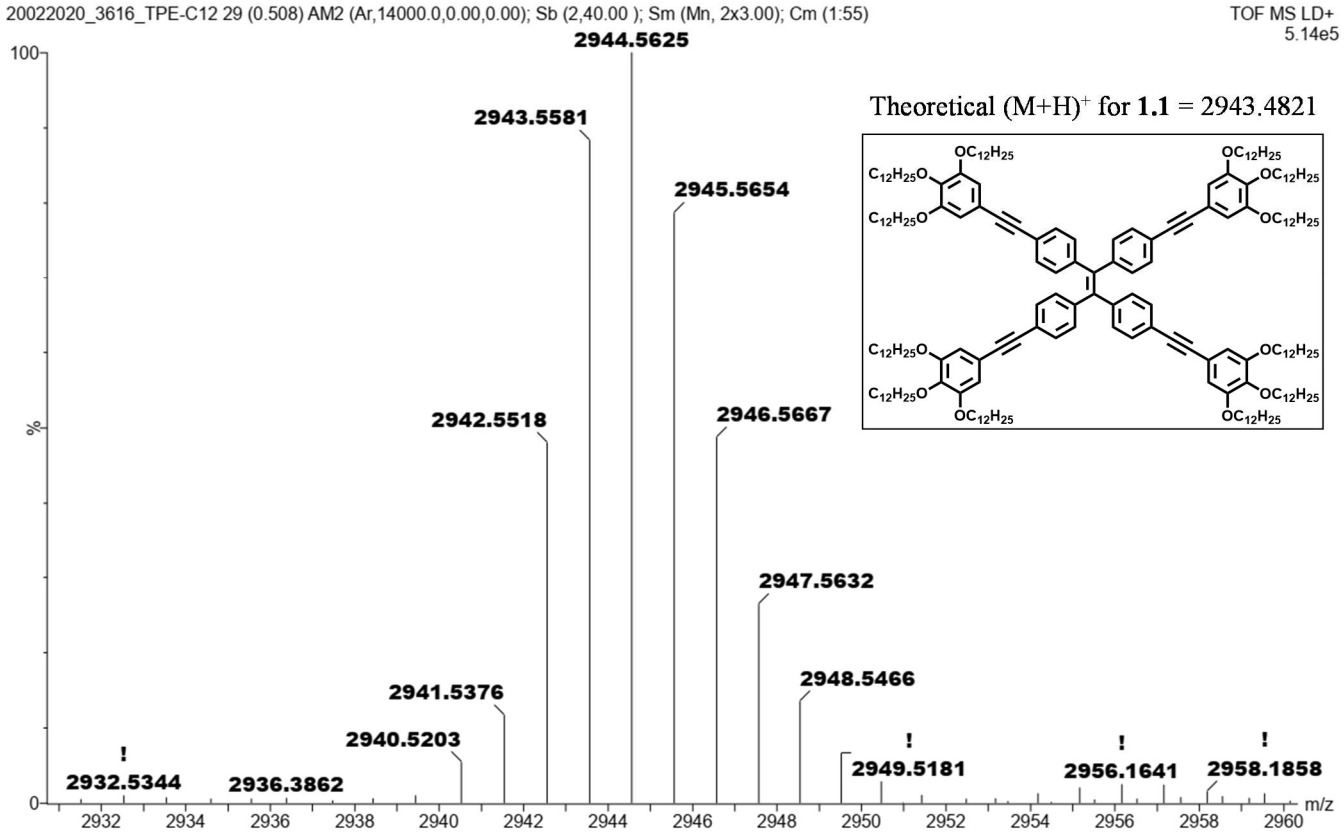

Synthesis of 1,1,2,2-tetrakis(4-((3,4,5-tris(tetradecyloxy)phenyl)ethynyl)phenyl)ethene (1.2):

Compound **1.2** was prepared by following same procedure as used in synthesizing **1.1**. The target material (**1.2**) was purified by using column chromatography (neutral alumina, Ethylacetate/Hexane (0.7:99.3)) to get the product as yellow solid (yield: 84 %).

^{1}H NMR (400 MHz, $CDCl_3$, δ ppm): 7.28 (d, J = 8.32 Hz, 8H), 7.00 (d, J = 8.24 Hz, 8H), 6.70 (s, 8H), 3.96 (t, J = 6.44 Hz, 24H), 1.83-1.72 (m, 24H), 1.49-1.42 (m, 24H), 1.36-1.25 (m, 240H), 0.88 (t, J = 6.70 Hz, 36H).

^{13}C NMR (100 MHz, $CDCl_3$, δ ppm): 153.14, 143.03, 141.04, 139.31, 131.57, 131.25, 122.01, 117.67, 110.27, 90.67, 88.18, 73.69, 69.29, 32.09, 30.49, 29.91, 29.87, 29.83, 29.80, 29.76, 29.56, 29.53, 29.50, 26.25, 22.85, 14.27.

IR (Neat, KBr, ν_{max}/cm^{-1}): 2955.20, 2923.55, 2853.41, 1573.83, 1507.45, 1467.48, 1419.28, 1354.32, 1259.36, 1234.01, 1117.81, 831.17, 748.74, 721.68.

MALDI-MS: *m/z* calcd for $C_{226}H_{373}O_{12}$ $(M+H)^+$: 3279.8577. Found: 3279.8394.

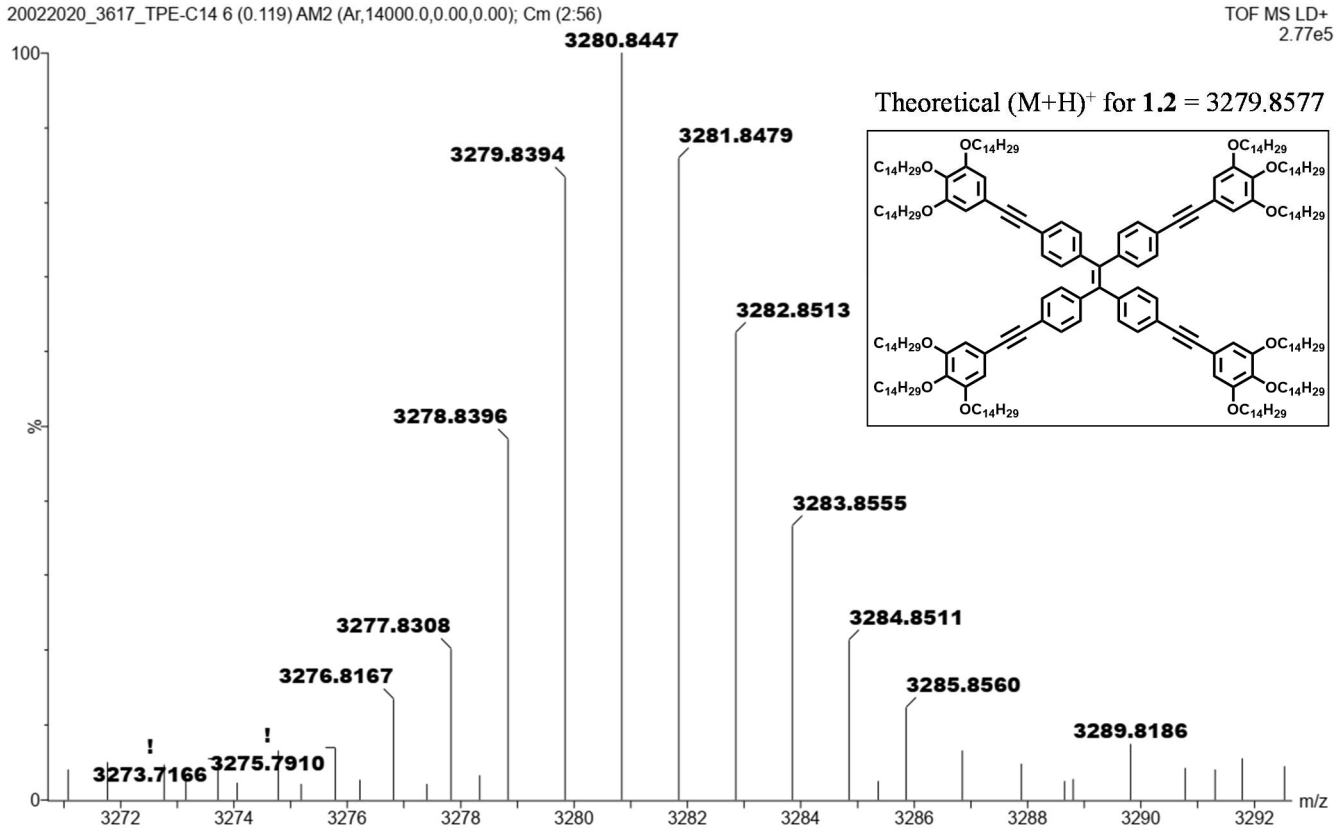

Synthesis of 1,1,2,2-tetrakis(4-((3,4,5-tris(hexadecyloxy)phenyl)ethynyl)phenyl)ethene (1.3):

Compound **1.3** was prepared by following same procedure as used in synthesizing **1.1**. The target material (**1.3**) was purified by using column chromatography (neutral alumina, Ethylacetate/Hexane (0.7:99.3)) to get the product as yellow solid (yield: 82 %). In ^{1}H NMR spectra of **1.3** one broad singlet (bs) peak is observed at 7.28 ppm, whereas in case of **1.1** and **1.2** at 7.28 ppm the signal is perceived as doublet.

^{1}H NMR (400 MHz, $CDCl_3$, δ ppm): 7.28 (bs, 8H), 6.99 (d, J = 7.64 Hz, 8H), 6.70 (s, 8H), 3.96 (t, J = 5.74 Hz, 24H), 1.80-1.71 (m, 24H), 1.48-1.42 (m, 24H), 1.34-1.23 (m, 288H), 0.87 (t, J = 5.68 Hz, 36H).
^{13}C NMR (100 MHz, $CDCl_3$, δ ppm): 153.13, 143.03, 141.03, 139.24, 131.57, 131.25, 122.00, 117.66, 110.20, 90.67, 88.18, 73.68, 69.25, 32.09, 30.48, 30.19, 30.11, 29.88, 29.84, 29.81, 29.76, 29.57, 29.54, 29.49, 26.25, 22.85, 14.28.
IR (Neat, KBr, ν_{max}/cm^{-1}): 2954.30, 2918.95, 2850.98, 1573.70, 1508.80, 1467.97, 1419.75, 1354.25, 1259.91, 1233.70, 1119.06, 831.54, 748.77, 721.88.
MALDI-MS: *m/z* calcd for $C_{250}H_{421}O_{12}$ $(M+H)^+$: 3616.2333. Found: 3616.2258.

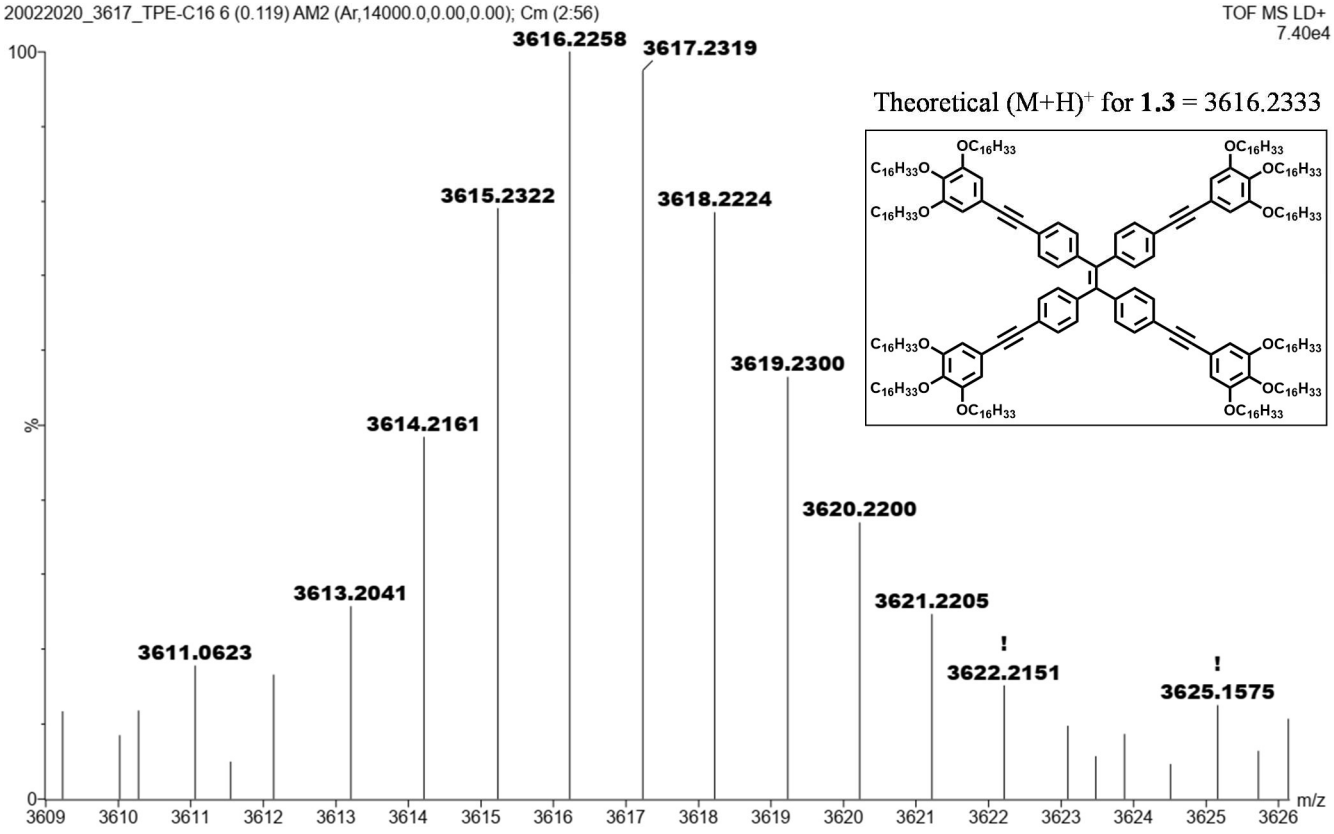
20022020_3617_TPE-C16 6 (0.119) AM2 (Ar,14000.0,0.00,0.00); Cm (2:56)
TOF MS LD+
7.40e4
100
%
0
3616.2258
3617.2319
3615.2322
3618.2224
3619.2300
3614.2161
3620.2200
3613.2041
3621.2205
3611.0623
3622.2151
3625.1575
m/z
3609
3610
3611
3612
3613
3614
3615
3616
3617
3618
3619
3620
3621
3622
3623
3624
3625
3626
Theoretical (M+H)+ for 1.3 = 3616.2333
OC16H33
C16H33O

3) NMR spectra:

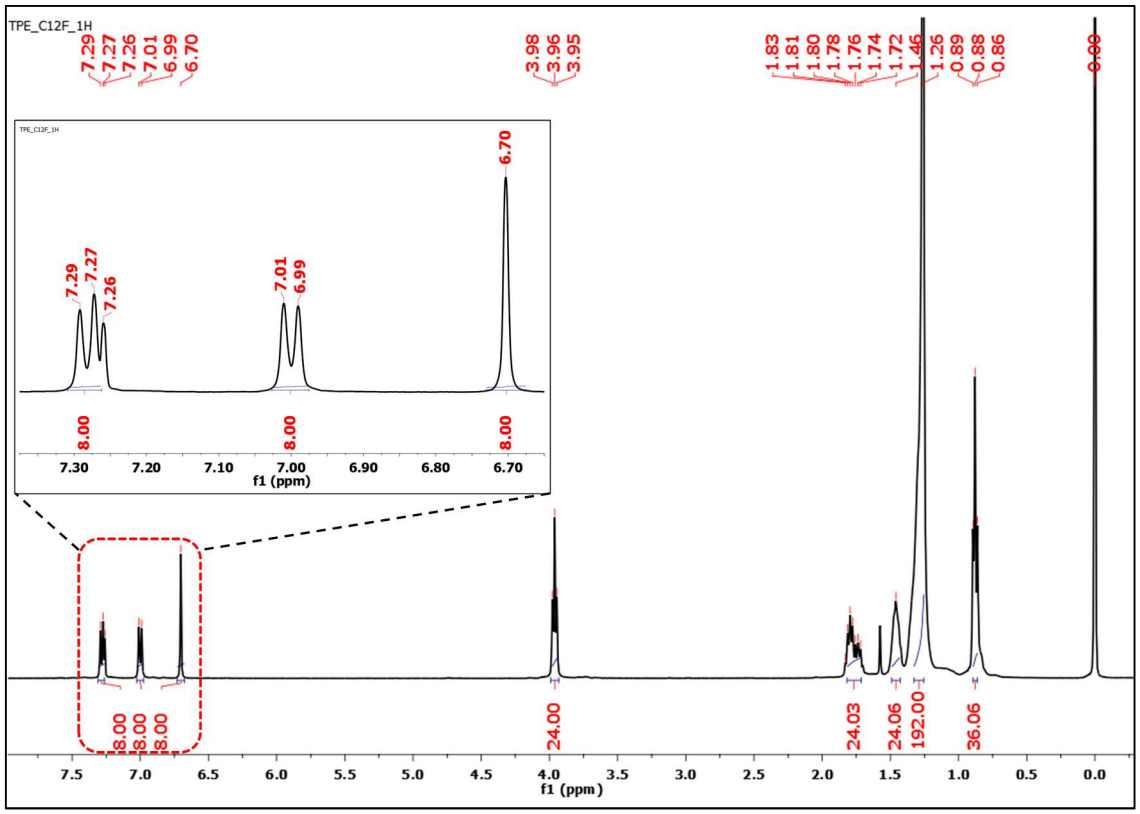

Fig. S1 ^{1}H NMR of 1,1,2,2-tetrakis(4-((3,4,5-tris(dodecyloxy)phenyl)ethynyl)phenyl)ethene (**1.1**).

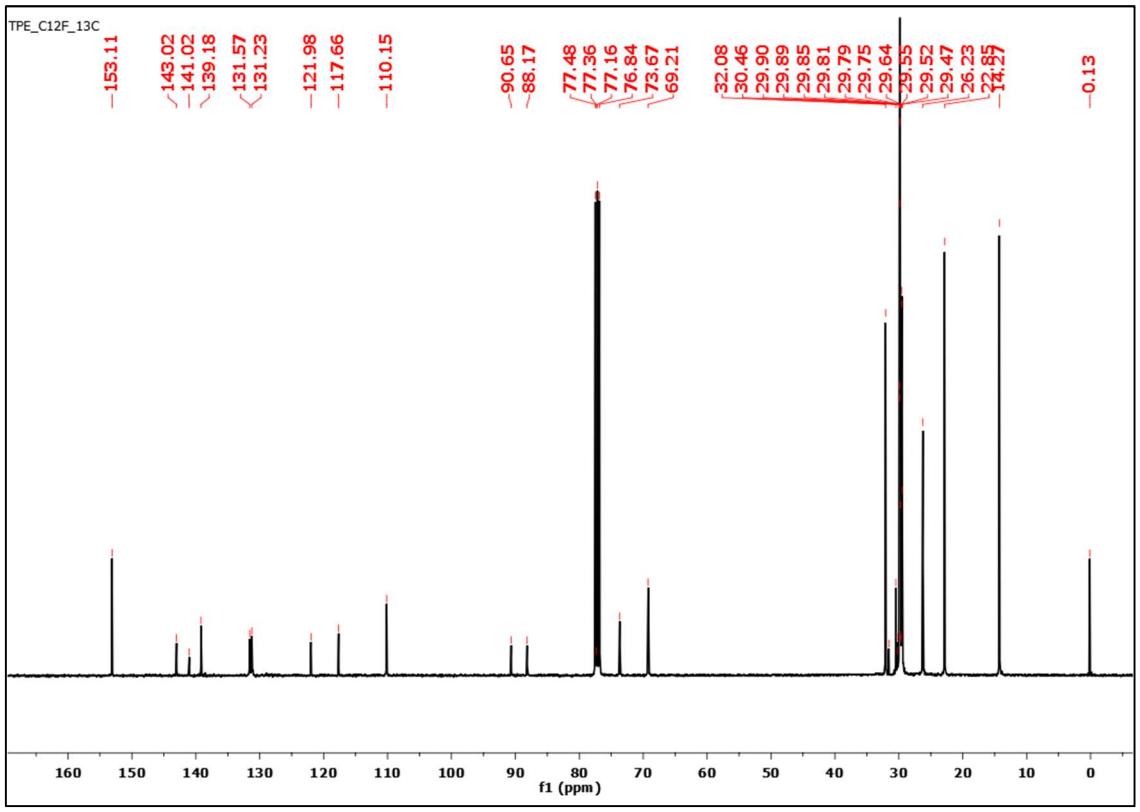

Fig. S2 ^{13}C NMR of 1,1,2,2-tetrakis(4-((3,4,5-tris(dodecyloxy)phenyl)ethynyl)phenyl)ethene (**1.1**).

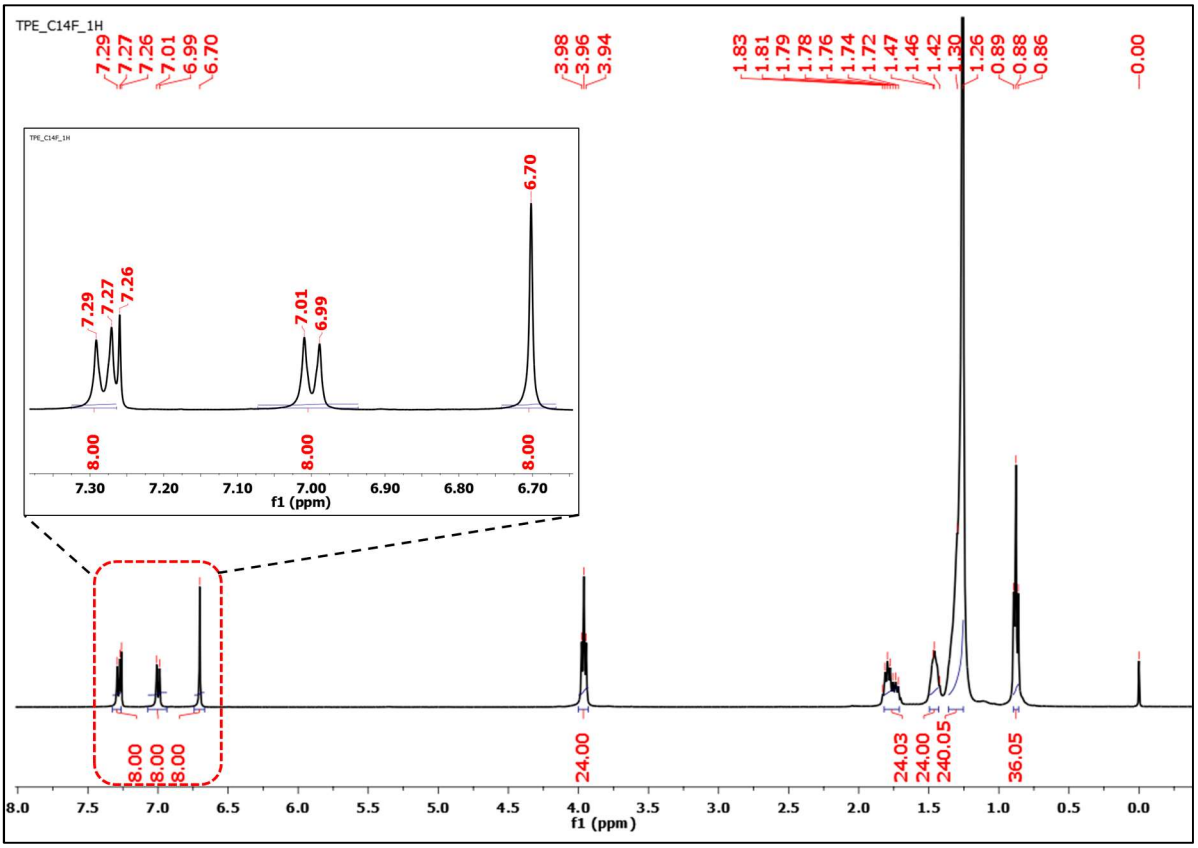

Fig. S3 ^{1}H NMR of 1,1,2,2-tetrakis(4-((3,4,5-tris(tetradecyloxy)phenyl)ethynyl)phenyl)ethene (**1.2**).

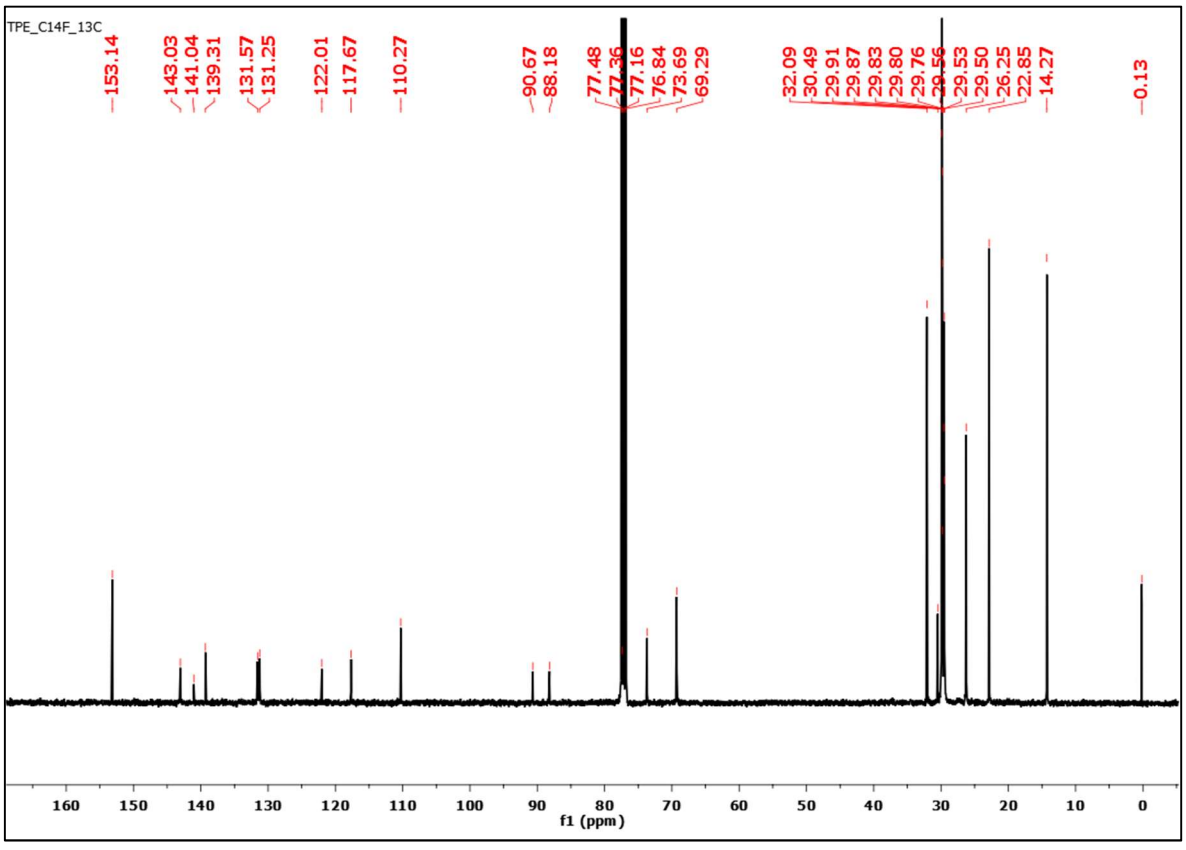

Fig. S4 ^{13}C NMR of 1,1,2,2-tetrakis(4-((3,4,5-tris(tetradecyloxy)phenyl)ethynyl)phenyl)ethene (**1.2**).

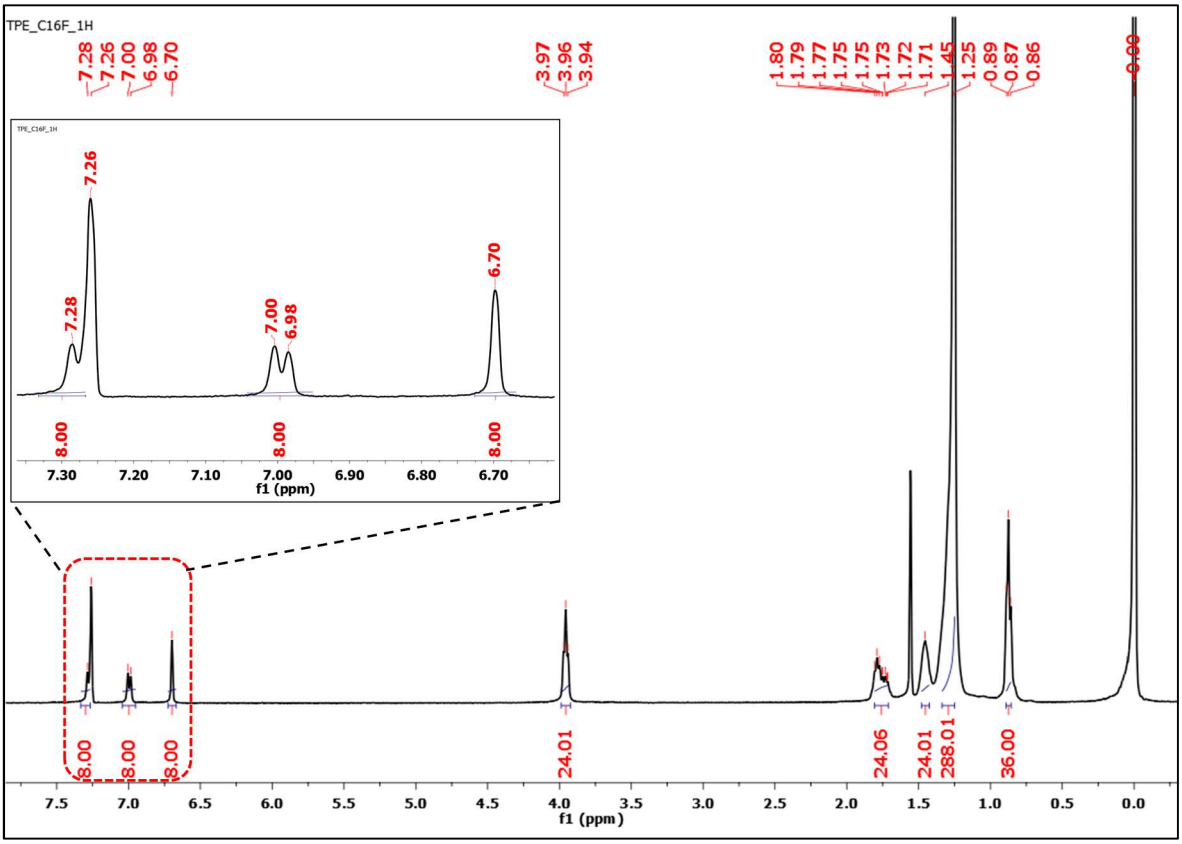

Fig. S5 ^{1}H NMR of 1,1,2,2-tetrakis(4-((3,4,5-tris(hexadecyloxy)phenyl)ethynyl)phenyl)ethene (**1.3**).

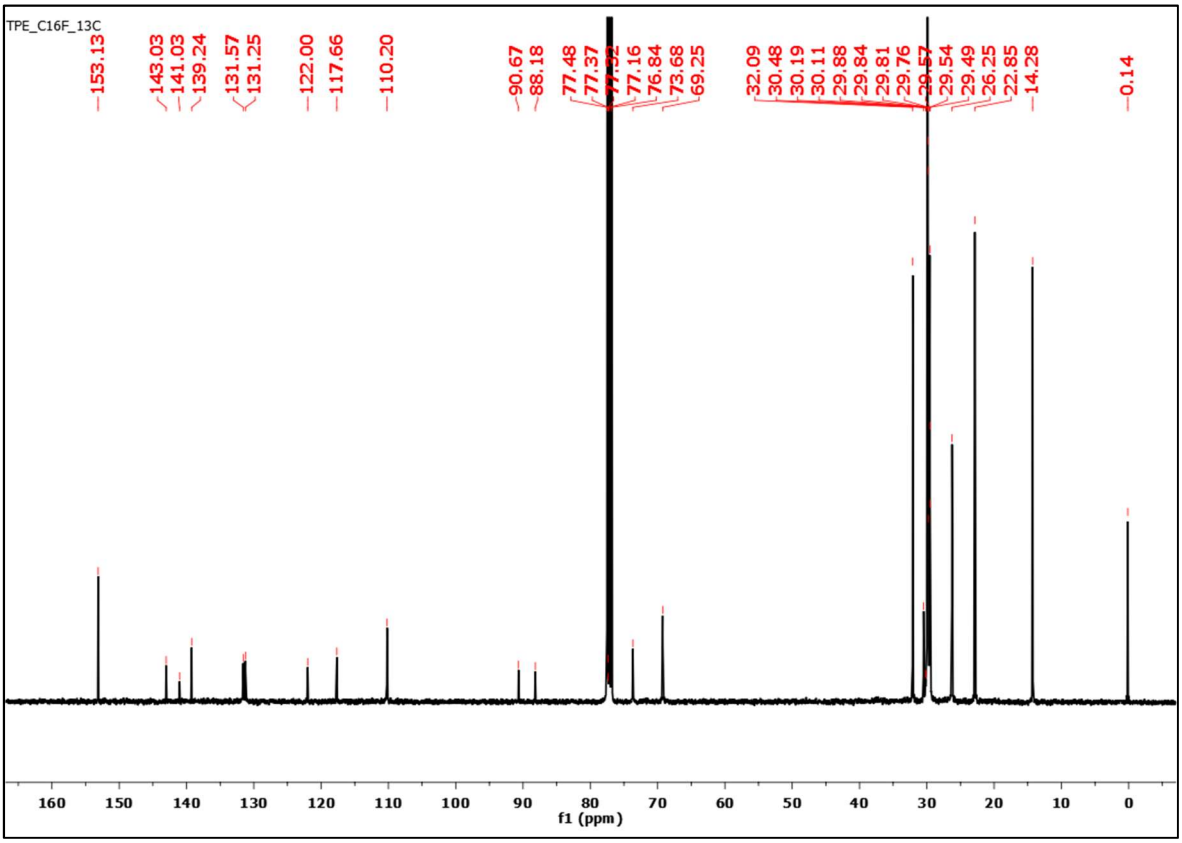

Fig. S6 ^{13}C NMR of 1,1,2,2-tetrakis(4-((3,4,5-tris(hexadecyloxy)phenyl)ethynyl)phenyl)ethene (**1.3**).

4) TGA curves:

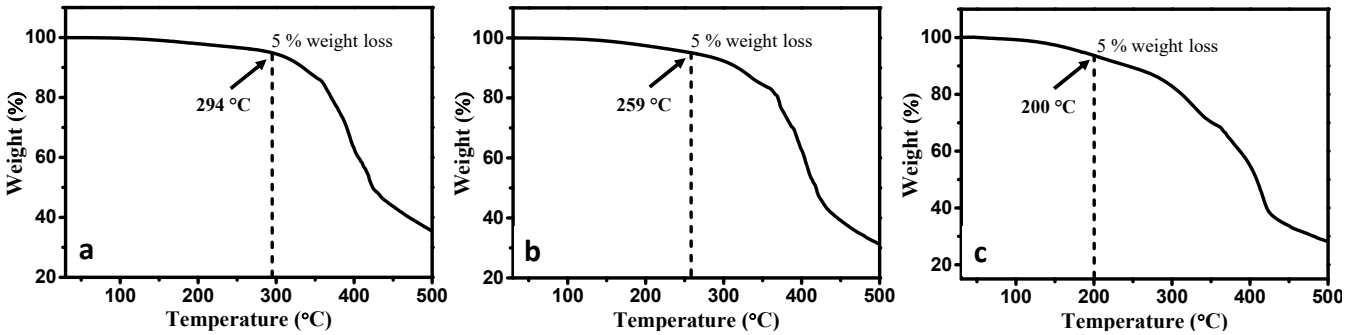

Fig. S7 TGA curves of (a) **1.1**, (b) **1.2** and (c) **1.3**. The measurements were performed under a nitrogen atmosphere, with heating and cooling rates of 10 °C/min.

5) DSC thermograms :

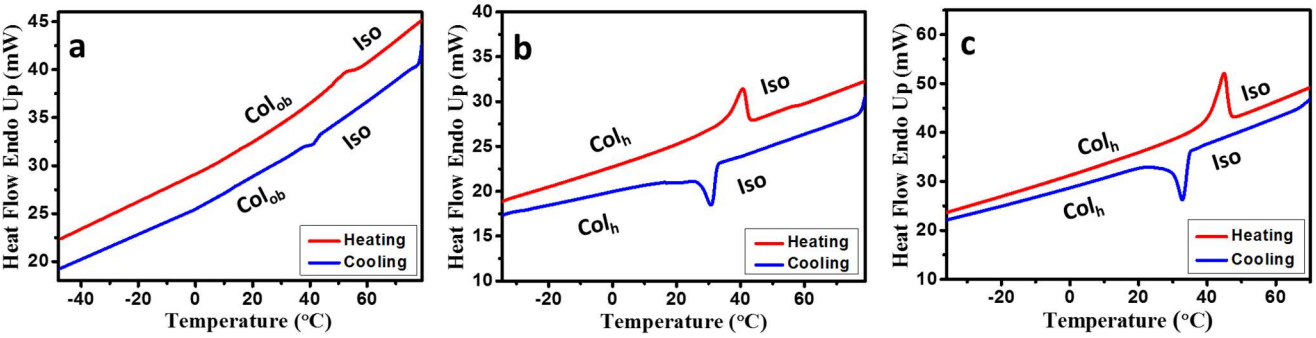

Fig. S8 DSC thermograms of compound (a) **1.1**, (b) **1.2** and (c) **1.3**. All the cooling and heating cycles were measured at the rate of 10 °C/min.

Table S1 Experimental data of thermal properties of compounds **1.1 – 1.3.**[a,b]

Mesogen	Heating Scan	Cooling Scan
1.1	Col_{ob} 52.1 (12.43) I	I 43.2 (9.30) Col_{ob}
1.2	Col_h 40.6 (20.28) I	I 30.6 (22.78) Col_h
1.3	Col_h 46.6 (32.54) I	I 34.8 (31.24) Col_h

[a] Transition temperatures (peak, in °C) and associated enthalpy changes in brackets in kJ mol^{-1}. [b] Transition temperatures from DSC. Abbreviations: Col_{ob} = Columnar oblique, Col_h = Columnar hexagonal, I = Isotropic liquid.

6) POM studies:

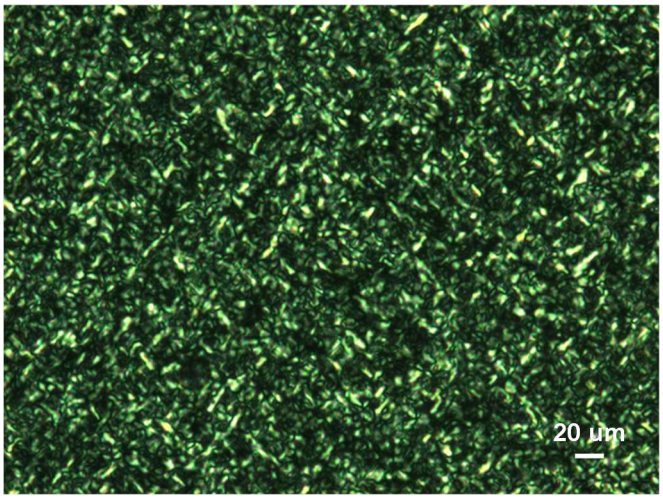

Fig. S9 Polarizing optical micrograph of compound **1.3** at 24.5 °C on cooling from isotropic phase (magnification X 200).

7) X-ray diffraction studies:

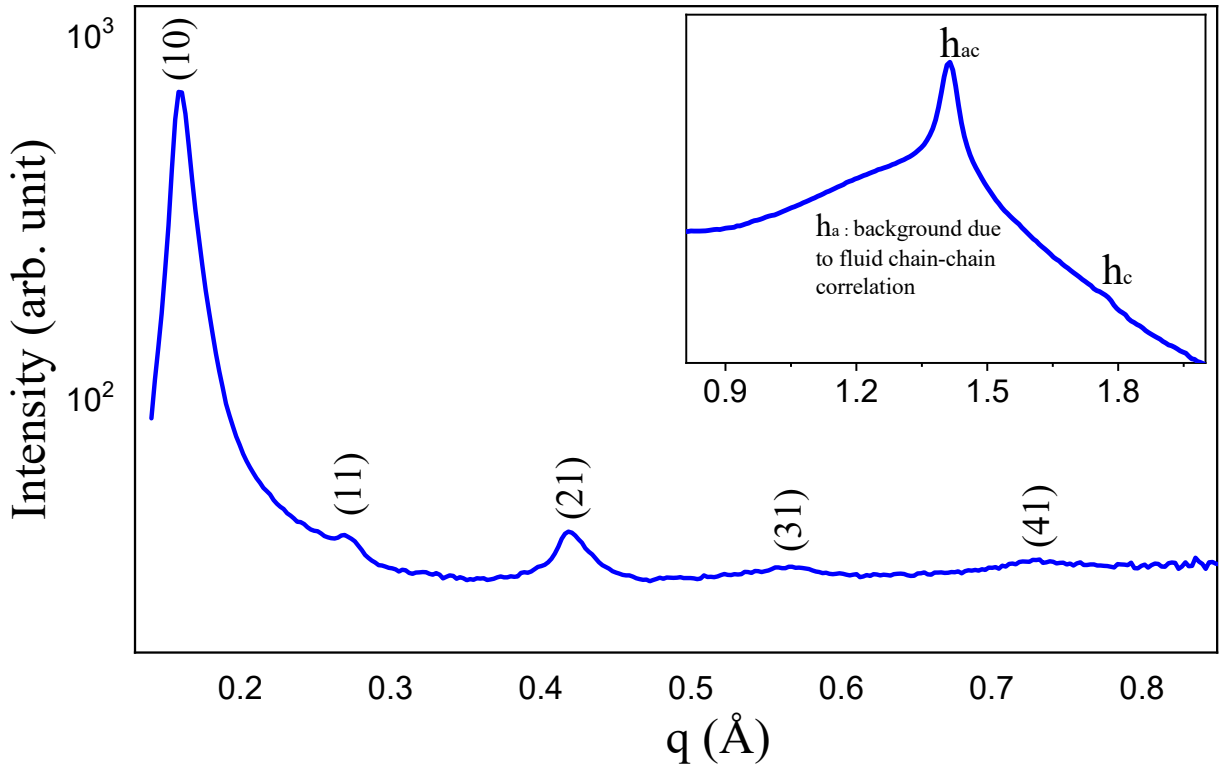

Fig. S10 Small angle and wide angle (inset) X-ray diffraction pattern with indexing of compound **1.3** at 25 °C on cooling from isotropic liquid.

Table S2 The observed and calculated *d*-spacings and planes of the diffraction peaks of the oblique lattice observed in compound **1.1** at 25 °C. The lattice parameters are a = 58.38 Å, b = 43.65 Å and α = 40.42°. h_a is due to chain-chain correlation. h_c due to core to core (face to face) correlations and correspond to the effective thickness of the disc. d_{obs}: experimental *d*-spacing; d_{cal}: calculated *d*-spacing by using the relation: $\frac{1}{d_{cal}^2} = \frac{1}{Sin^2\alpha}\left[\frac{h^2}{a^2} + \frac{k^2}{b^2} - \frac{2\,h\,k\,Cos\alpha}{a\,b}\right]$; h, k are the Miller indices of the reflections corresponding to the columnar oblique phase; a, b and α are the unit cell parameters with α is the angle.

(hk)	***d-spacing Experimental d_{obs} (Å)***	***d-spacing Calculated d_{cal} (Å)***	***Relative Intensity I(hk)***	***Multiplicity***	***Phase Φ(hk)***
10	37.85	37.85	100.00	2	0
01	28.30	28.30	3.11	2	π
22	21.82	21.82	2.78	2	π
20	18.81	18.92	3.20	2	π
31	17.31	17.50	2.10	2	π
h_a	4.84	-			
h_c	3.53	-			

Table S3 The observed and calculated *d*-spacings and planes of the diffraction peaks of the hexagonal lattice observed in compound **1.2** at 25 °C. The lattice parameter is a = 45.34 Å. h_{ac} peak is indicative of partial crystalized alkyl chains and h_c peak is due to core to core (face to face) correlations. d_{obs}: experimental *d*-spacing; d_{cal}: calculated *d*-spacing by using the relation: $\frac{1}{d^2} = \frac{4}{3}\left(\frac{h^2+h\,k+k^2}{a^2}\right)$; h, k are the Miller indices.

(hk)	***d-spacing Experimental d_{obs} (Å)***	***d-spacing Calculated d_{cal} (Å)***	***Relative Intensity I(hk)***	***Multiplicity***	***Phase Φ(hk)***
10	39.27	39.27	100.00	6	0
11	22.70	22.67	2.72	6	π
21	14.64	14.84	1.81	12	0
31	10.72	10.89	1.93	12	π
h_{ac}	4.50	-			
h_c	3.53	-			

Table S4 The observed and calculated *d*-spacings and planes of the diffraction peaks of the hexagonal lattice observed in compound **1.3** at 25 °C. The lattice parameter is a = 45.34 Å. h_{ac} peak is indicative of partial crystalized alkyl chains and h_c peak is due to core to core (face to face) correlations. d_{obs}: experimental *d*-spacing; d_{cal}: calculated *d*-spacing by using the relation: $\frac{1}{d^2} = \frac{4}{3}\left(\frac{h^2+h\,k+k^2}{a^2}\right)$; h, k are the Miller indices.

(hk)	***d-spacing Experimental d_{obs} (Å)***	***d-spacing Calculated d_{cal} (Å)***	***Relative Intensity I(hk)***	***Multiplicity***	***Phase Φ(hk)***
10	39.27	39.27	100.00	6	0

11	22.77	22.67	4.45	6	π
21	14.89	14.84	6.17	12	0
31	10.95	10.89	4.88	12	0
41	8.58	8.57	5.02	12	π
$\mathbf{h_{ac}}$	4.44	-			
$\mathbf{h_c}$	3.53	-			

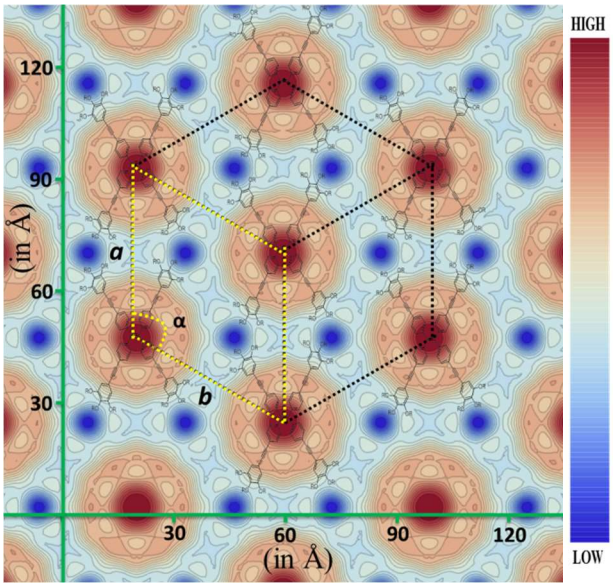

Fig. S11 Electron density map in the columnar hexagonal phase of compound **1.3** at 25 °C. Hexagon showed the conventional unit cell of the Col_h lattice and there are three primitive unit cells within this conventional unit cell. *a*, *b* and α are the lattice parameters with *a* = b and α equal to 120°. Deep red represents the highest electron density and deep blue is the lowest.

8) Photophysical and mechanochromic studies:

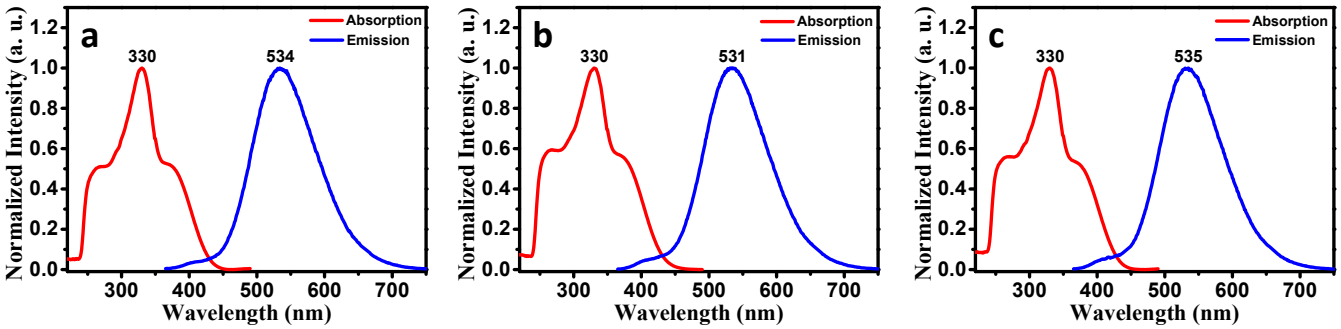

Fig. S12 UV-vis absorption and PL emission spectra of compounds (a) **1.1**, (b) **1.2** and (c) **1.3** in tetrahydrofuran (THF) solvent of 10^{-6} M concentration.

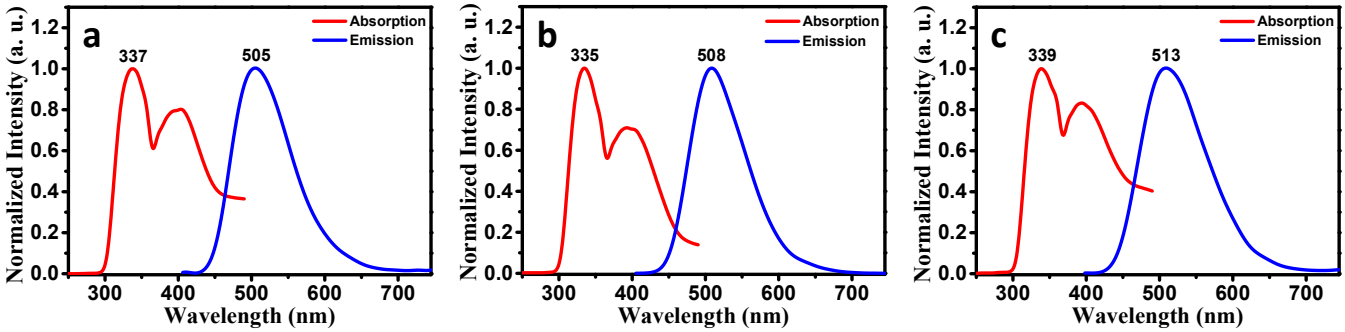

Fig. S13 UV-vis absorption and PL emission spectra of compounds (a) **1.1**, (b) **1.2** and (c) **1.3** in solid state.

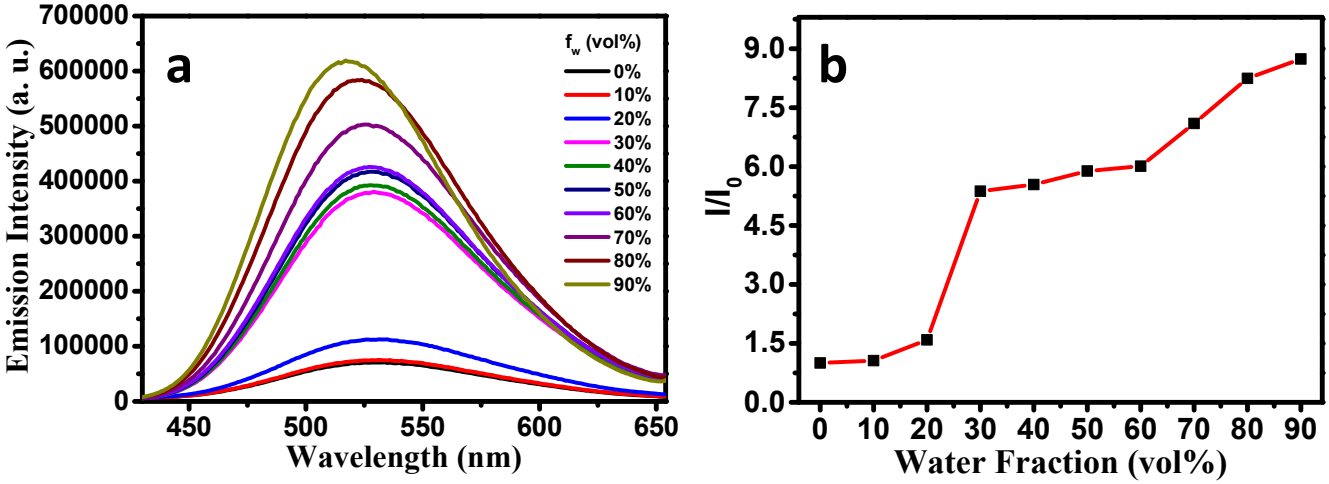

Fig. S14 (a) PL spectra of TPE-derivative **1.1** with different water fractions, f_w (vol %). (b) Plot of I/I_0 vs water fraction (f_w), where I_0 represents the intensity of emission in solution of THF only and I belongs to the intensity of emission with increasing amount of f_w.

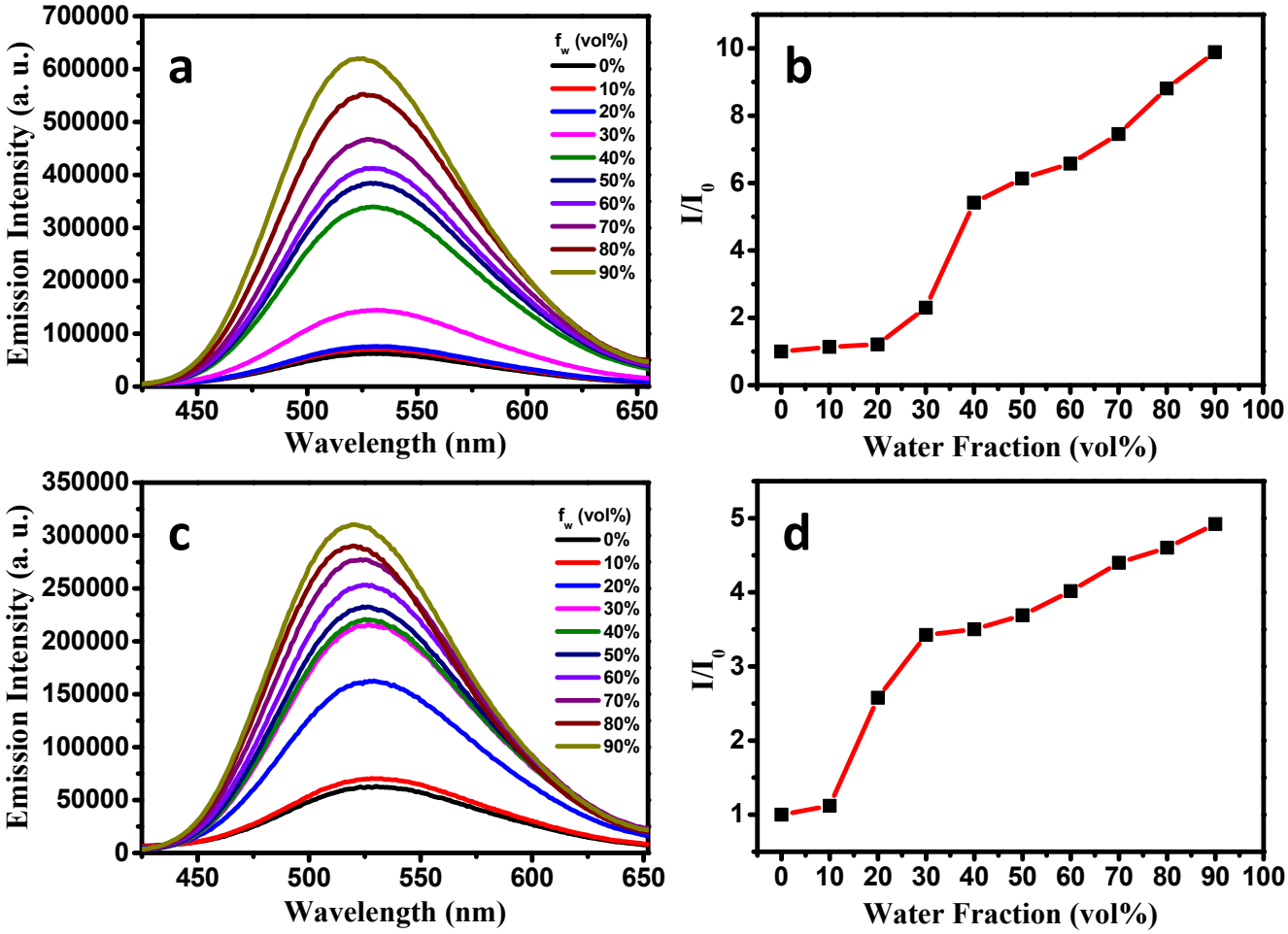

Fig. S15 PL spectra of (a) **1.2** and (c) **1.3** with different water fractions, f_w (vol %). Plot of I/I_0 vs water fraction (f_w) of (b) **1.2** and (d) **1.3**, where I_0 represents the intensity of emission in solution of THF only and I belongs to the intensity of emission with increasing amount of f_w.

All the TPE-based columnar mesogens (**1.1-1.3**) having variations with only peripheral alkyl chains exhibited aggregation-induced emission (AIE) behavior. This implies that here the central TPE core is mainly responsible for AIE effect. In solution the propeller shaped TPE unit undergoes intramolecular rotation which resulted in quenching of luminescence, whereas it exhibits the restricted intramolecular rotations at aggregated state resulting in significant increase in emission intensity.[3-7] Additionally, the peripheral alkyl chains of the TPE-based DLCs (**1.1-1.3**) enhanced their aggregation capabilities by decreasing the solubility in THF/water solution.[8,9]

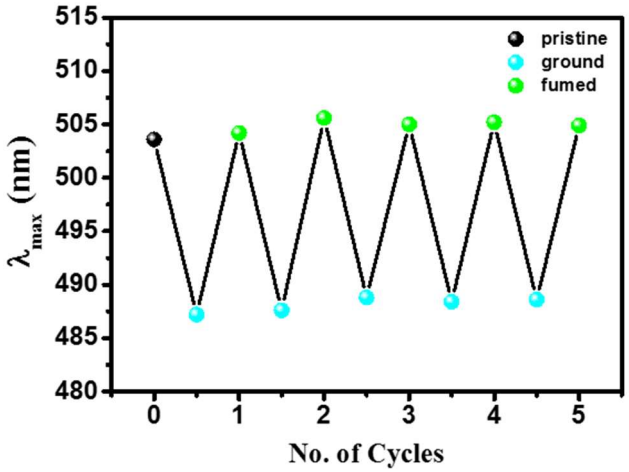

Fig. S16 Repeated switching in wavelength of emission maxima (λ_{max}) of compound **1.1** upon mechanical grinding and subsequently fumed with dichloromethane in 5 cycles.

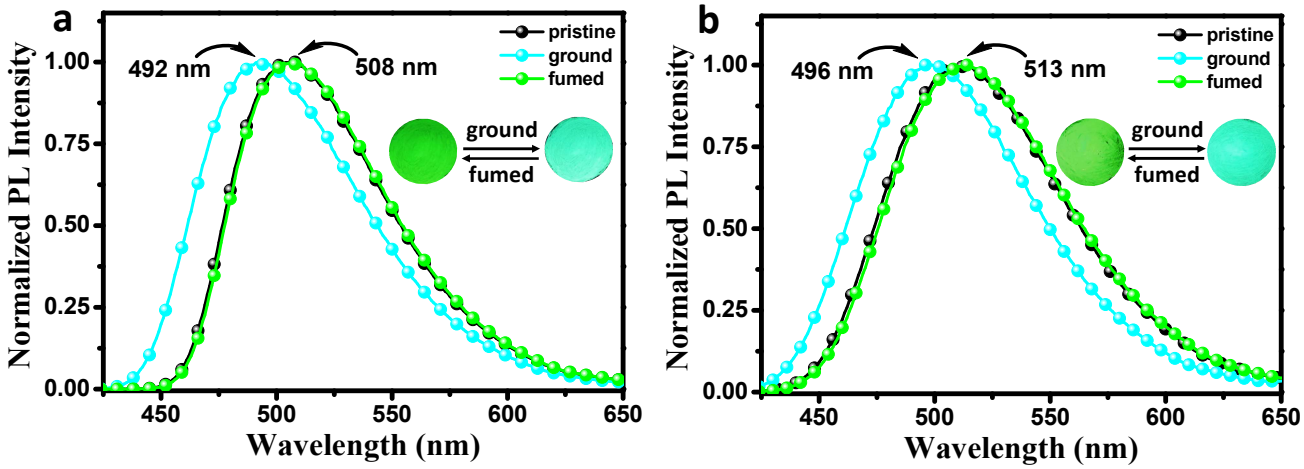

Fig. S17 Shifting of emission maxima in PL spectra of (a) **1.2** and (b) **1.3** before and after grinding, also after exposing it to dichloromethane vapours (λ_{ex} = 335 nm for **1.2** and λ_{ex} = 339 nm for **1.3**). Inset shows the corresponding images with different conditions under UV light.

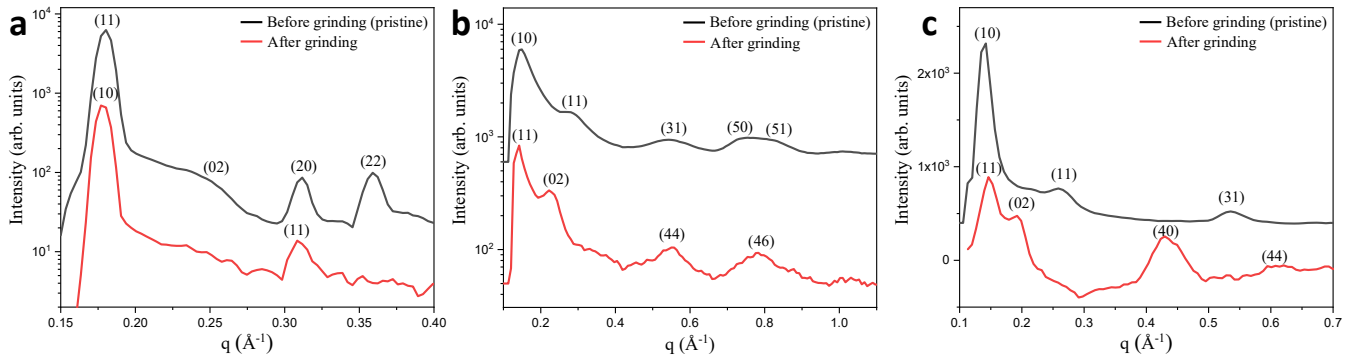

Fig. S18 X-ray diffraction pattern of (a) **1.1**, (b) **1.2** and (c) **1.3** with indexing: black color exhibiting diffraction pattern before grinding and red color displaying diffraction pattern after grinding.

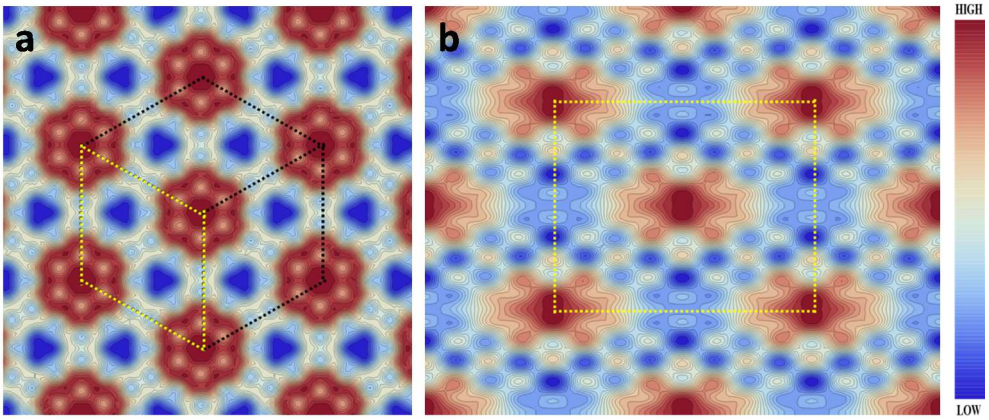

Fig. S19 Electron density map of **1.2** (a) before grinding, exhibiting Col_h and (b) after grinding, exhibiting centered Col_r assembly. Unit cell is shown in the dotted yellow boundary. Deep red correspond to highest electron density and deep blue is the lowest.

Table S5 The observed and calculated d-spacings and the corresponding index of the planes of the diffraction peaks of the oblique lattice (before grinding) of compound **1.1**. d_{obs}: experimental *d*-spacing; d_{cal}: calculated *d*-spacing by using the relation: $\frac{1}{d^2_{cal}} = \frac{1}{Sin^2\alpha}\left[\frac{h^2}{a^2} + \frac{k^2}{b^2} - \frac{2\,h\,k\,Cos\alpha}{a\,b}\right]$; *h*, *k* are the Miller indices of the reflections; *a*, *b* and α are the unit cell parameters. The lattice parameters are *a* = 41.30 Å, *b* = 50.76 Å and α = 78.04°.

(hk)	***d-spacing Experimental d_{obs} (Å)***	***d-spacing Calculated d_{cal} (Å)***
11	35.10	35.10
02	24.83	24.83
20	20.20	20.20
22	17.51	17.55

Table S6 The observed and calculated d-spacings and the corresponding index of the planes of the diffraction peaks of the hexagonal lattice (after grinding) of compound **1.1**. d_{obs}: experimental *d*-spacing; d_{cal}: calculated *d*-spacing by using the relation: $\frac{1}{d^2} = \frac{4}{3}\left(\frac{h^2+h\,k+k^2}{a^2}\right)$; *h*, *k* are the Miller indices. The lattice parameter is *a* = 41.02 Å.

(hk)	***d-spacing Experimental d_{obs} (Å)***	***d-spacing Calculated d_{cal} (Å)***
10	35.52	35.52
11	20.41	20.51

Table S7 The observed and calculated d-spacings and the corresponding index of the planes of the diffraction peaks of the hexagonal lattice (before grinding) of compound **1.2**. d_{obs}: experimental *d*-spacing; d_{dcal}: calculated *d*-spacing by using the relation: $\frac{1}{d^2} = \frac{4}{3}\left(\frac{h^2+h\,k+k^2}{a^2}\right)$; *h*, *k* are the Miller indices. The lattice parameter is *a* = 47.99 Å.

(hk)	*d-spacing Experimental d_{obs} (Å)*	*d-spacing Calculated d_{cal} (Å)*	*Relative Intensity I(hk)*	*Multiplicity*	*Phase Φ(hk)*
10	41.58	41.56	100.00	6	0
11	23.98	24.00	19.98	6	π
31	11.42	11.53	6.48	12	0
50	8.42	8.31	7.18	6	0
51	7.62	7.46	//	//	//

Table S8 The observed and calculated d-spacings and the corresponding index of the planes of the diffraction peaks of the centered rectangular lattice (after grinding) of compound **1.2**. d_{obs}: experimental *d*-spacing; d_{cal}: calculated *d*-spacing by using the relation:$\frac{1}{d^2} = (\frac{h^2}{a^2} + \frac{k^2}{b^2})$; *h*, *k* are the Miller indices, with $h + k = 2n, n\ is\ an\ integer$. The lattice parameters are *a* = 70.99 Å and *b* = 56.60 Å.

(hk)	*d-spacing Experimental d_{obs} (Å)*	*d-spacing Calculated d_{cal} (Å)*	*Relative Intensity I(hk)*	*Multiplicity*	*Phase Φ(hk)*
11	44.25	44.26	100.00	4	π
02	28.30	28.30	40.02	2	0
44	11.28	11.06	12.42	4	0
46	8.10	8.33	10.90	4	π

Table S9 The observed and calculated d-spacings and the corresponding index of the planes of the diffraction peaks of the hexagonal lattice (before grinding) of compound **1.3**. d_{obs}: experimental *d*-spacing; d_{cal}: calculated *d*-spacing by using the relation: $\frac{1}{d^2} = \frac{4}{3}(\frac{h^2+h\,k+k^2}{a^2})$; *h*, *k* are the Miller indices. The lattice parameter is *a* = 49.36 Å.

(hk)	*d-spacing Experimental d_{obs} (Å)*	*d-spacing Calculated d_{cal} (Å)*
10	42.74	42.75
11	24.71	24.68
31	11.80	11.86

Table S10 The observed and calculated d-spacings and the corresponding index of the planes of the diffraction peaks of the centered rectangular lattice (after grinding) of compound **1.3**. d_{obs}: experimental *d*-spacing; d_{cal}: calculated *d*-spacing by using the relation:$\frac{1}{d^2} = (\frac{h^2}{a^2} + \frac{k^2}{b^2})$; *h*, *k* are the Miller indices, with $h + k = 2n, n\ is\ an\ integer$. The lattice parameters are *a* = 57.66 Å, *b* = 64.44 Å.

(hk)	*d-spacing Experimental d_{obs} (Å)*	*d-spacing Calculated d_{cal} (Å)*
11	42.97	42.97
02	32.22	32.22
40	14.40	14.42
44	10.52	10.74

9) Electrochemical studies:

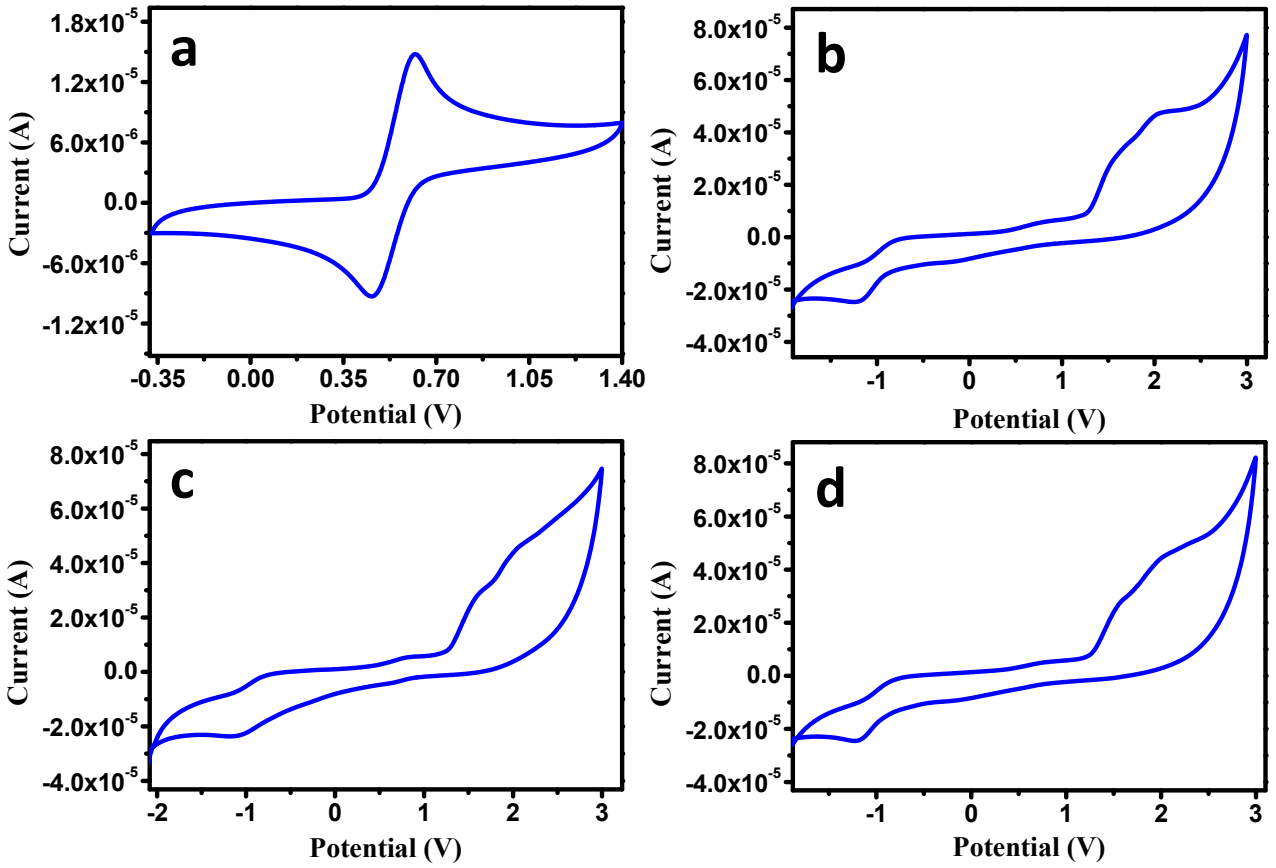

Fig. S20 Cyclic voltammograms of (a) ferrocene, and compounds (b) **1.1**, (c) **1.2** and (d) **1.3** in HPLC DCM solution of TBAP (0.1 M) at a scanning rate 50 mVs^{-1}.

Table S11 Electrochemical properties of compounds **1.1** - **1.3**.

Compound	E_{HOMO} (eV)	E_{LUMO} (eV)	$\Delta E_{g,CV}$ (eV)
1.1	-5.53	-3.39	2.14
1.2	-5.48	-3.43	2.05
1.3	-5.50	-3.38	2.12

10) Computational studies:

To understand the electronic properties and frontier molecular orbital energy level of compound **1.1-1.3** theoretical calculations were carried out with Gaussian 09 suite of packages.[10] A full optimization was carried out using the hybrid functional, Becke's three parameter exchange and the LYP Correlation Functional (B3LYP)[11] at a split valence basis set 6-31G(d,p). Both the HOMO and LUMO of the materials are located on the TPE core. The frontier molecular orbitals for the TPE derivatives are shown below.

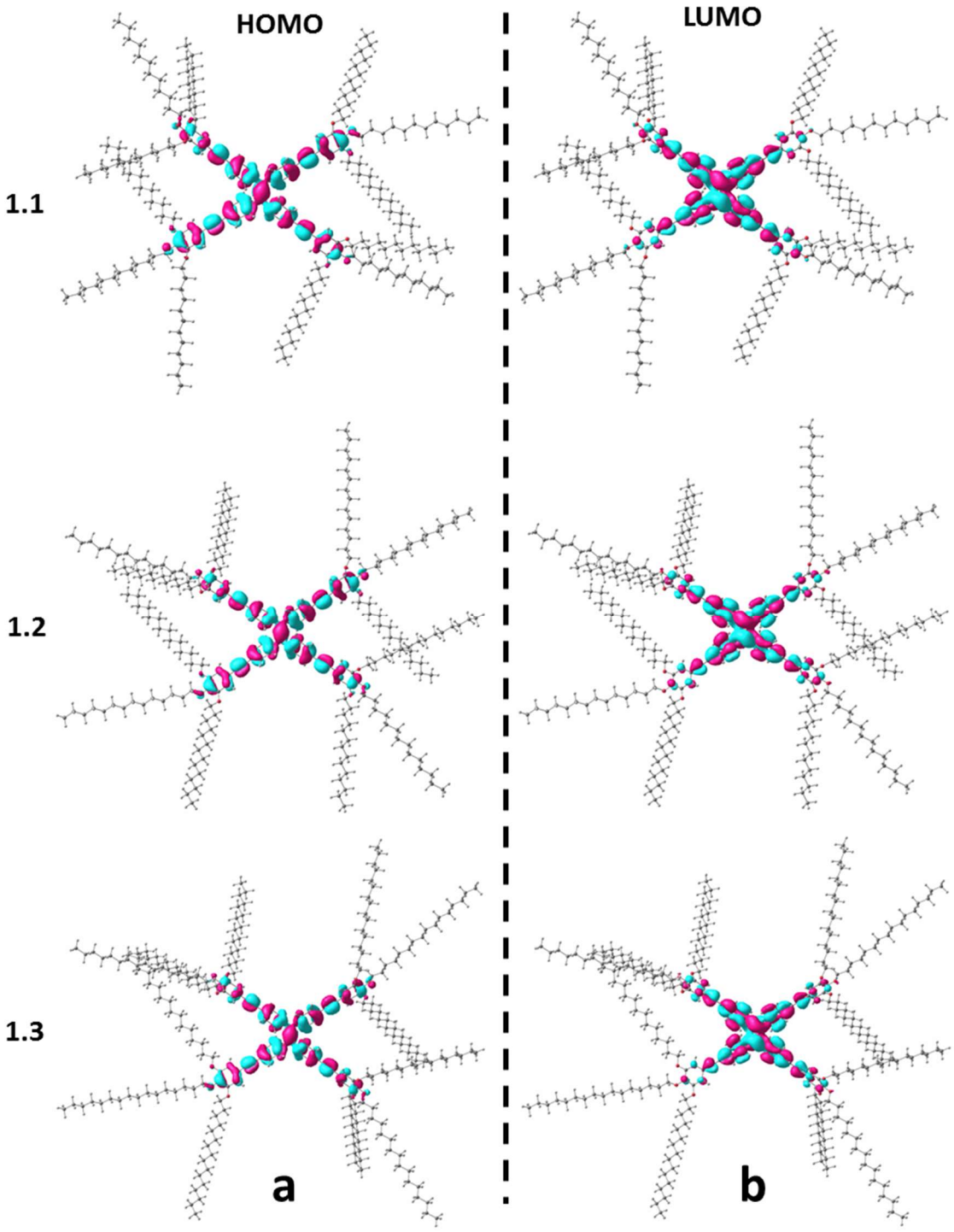

Fig. S21 Frontier molecular orbitals: (a) HOMO and (b) LUMO of compounds **1.1**, **1.2** and **1.3**.

11) OLED device fabrication:

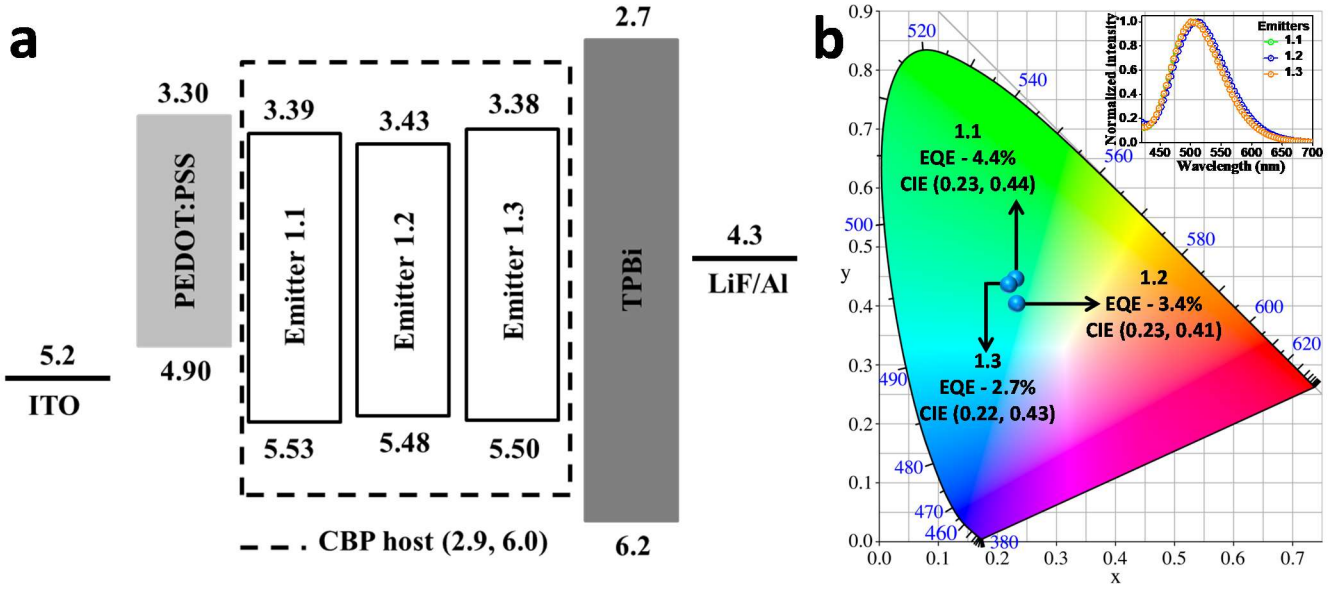

Fig. S22 (a) Schematic illustration of energy-level diagram of the solution-processed OLED devices comprising emitter **1.1-1.3** with CBP as a host matrix. (b) CIE chromatogram (inset shows EL spectra) of OLED devices consists of 3.0 wt% emitters (**1.1-1.3**) doped in CBP host.

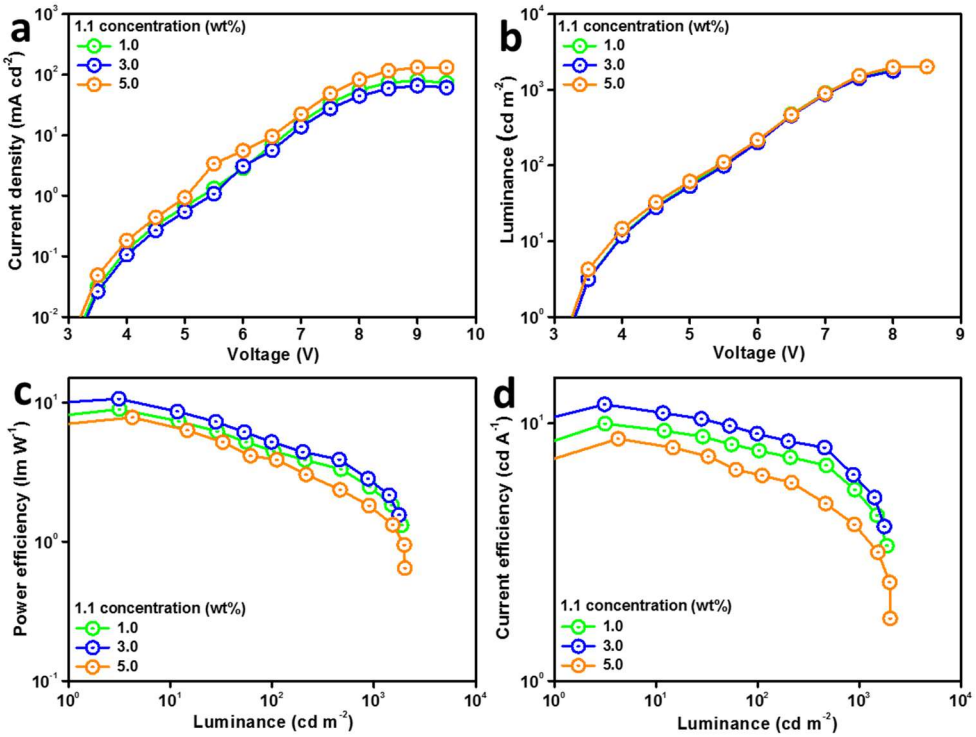

Fig. S23 (a) Current density-voltage, (b) luminance-voltage, (c) power efficiency-luminance and (d) current efficiency-luminance plots of the solution-processed OLED devices using CBP host with 1.0, 3.0, and 5.0 wt% **1.1** dopant concentration.

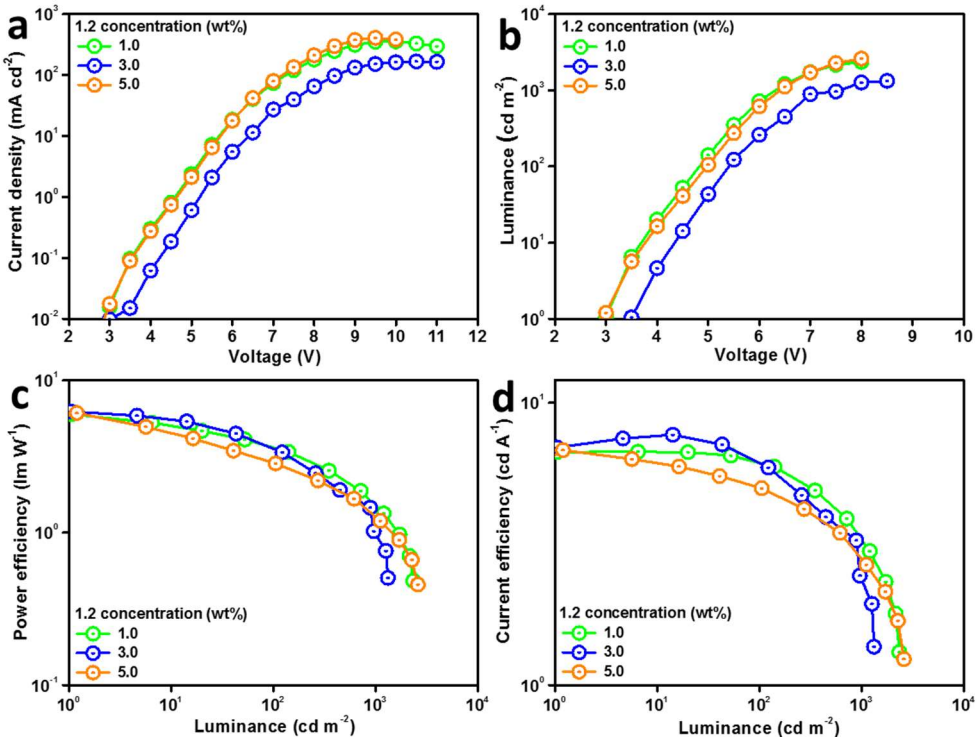

Fig. S24 (a) Current density-voltage, (b) luminance-voltage, (c) power efficiency-luminance and (d) current efficiency-luminance plots of the solution-processed OLED devices using CBP host with 1.0, 3.0, and 5.0 wt% **1.2** dopant concentrations.

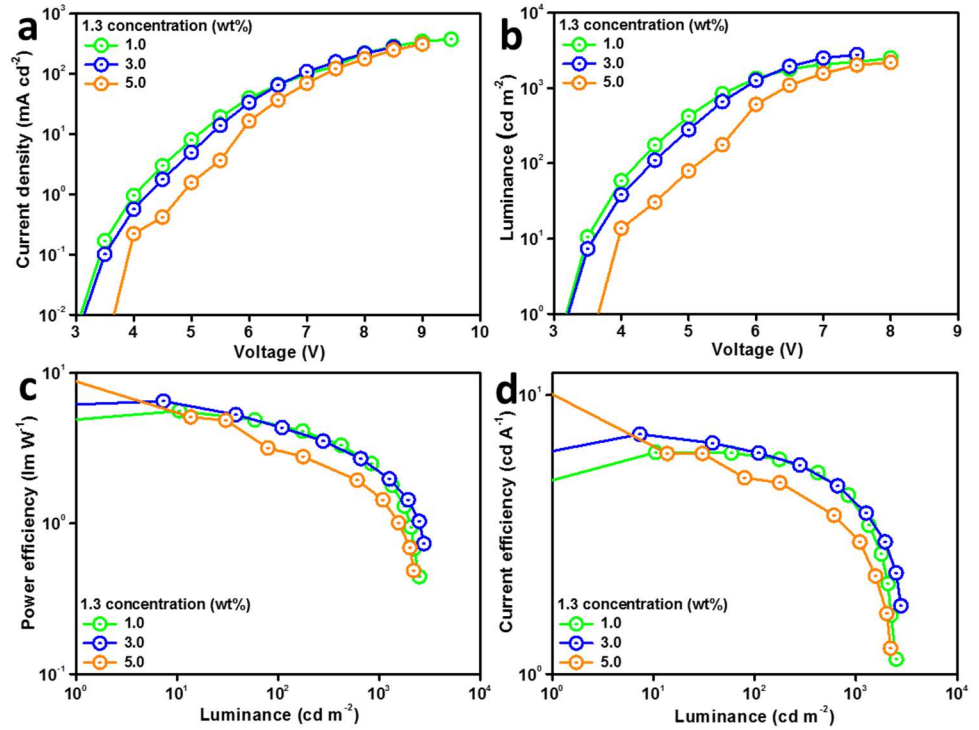

Fig. S25 (a) Current density-voltage, (b) luminance-voltage, (c) power efficiency-luminance and (d) current efficiency-luminance plots of the solution-processed OLED devices using CBP host with 1.0, 3.0, and 5.0 wt% **1.3** dopant concentrations.

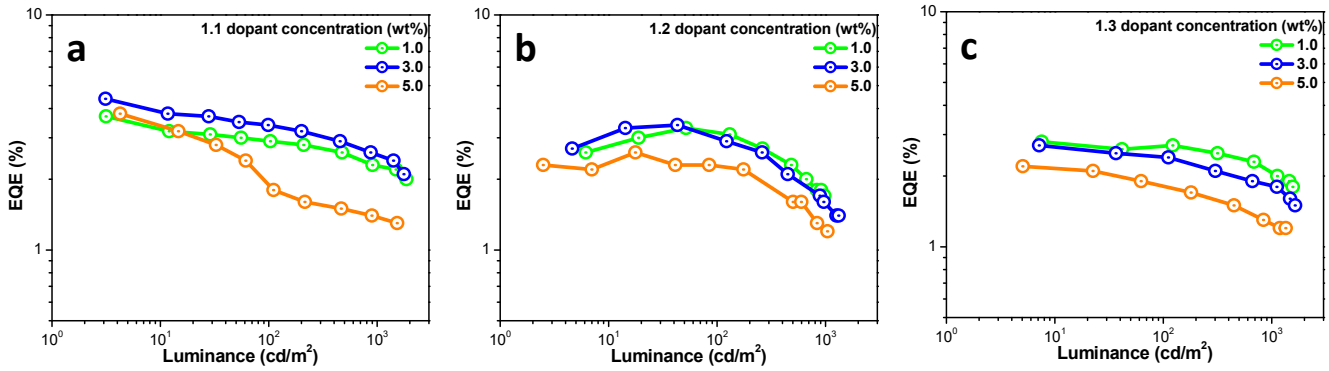

Fig. S26 EQE-luminance characteristics of the OLED devices based on emitter (a) **1.1**, (b) **1.2** and (c) **1.3** at various doping concentrations (1.0, 3.0 and 5.0 wt%) into CBP host.

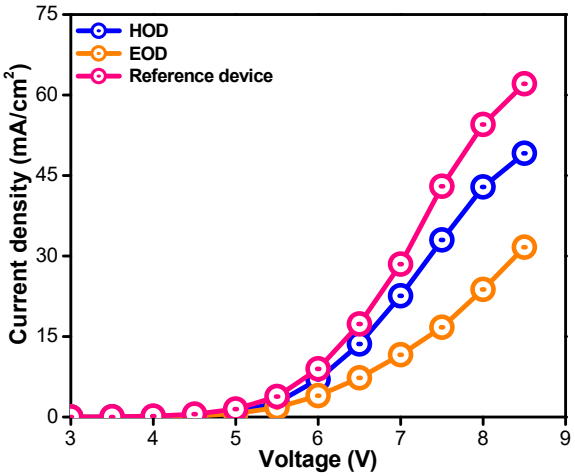

Fig. S27 Current density-voltage curves of hole-only device (HOD) and electron-only device (EOD) of **1.1** (100 wt%) compared with reference device (CBP:**1.1** 3.0 wt%).

Table S12 Effect of doping concentration on the power efficiency (PE), current efficiency (CE), external quantum efficiency (EQE), CIE coordinates and maximum luminance of solution-processed OLED devices with the CBP host for **1.1-1.3**.

Dopant	Dopant (wt%)	T_{on}[a] (V)	PE_{max}/ CE_{max}/ EQE_{max}[b] (lm W^{-1}/ cd A^{-1}/ %)	PE_{100}/ CE_{100}/ EQE_{100}[c] (lm W^{-1}/ cd A^{-1}/ %)	PE_{1000}/ CE_{1000}/ EQE_{1000}[d] (lm W^{-1}/ cd A^{-1}/ %)	CIE_{xy} Coordinates[e]	Max. Lum. (cd m^{-2})
1.1	1	3.1	8.9/ 10.1/ 3.7	4.5/ 7.9/ 2.9	2.4/ 5.4/ 2.3	(0.23, 0.44) / (0.22, 0.41)	1865
	3	3.1	10.6/ 11.8/ 4.4	5.2/ 9.1/ 3.4	2.7/ 6.0/ 2.6	(0.23, 0.44) / (0.22, 0.41)	1768
	5	3.1	7.8/ 8.7/ 3.8	2.4/ 4.0/ 1.7	1.7/ 3.9/ 1.2	(0.24, 0.45) / (0.24, 0.43)	2017
	100	-	- / - / -	- / - / -	- / - / -	- / -	7
1.2	1	3.5	6.0/ 6.7/ 3.3	3.7/ 6.2/ 3.1	1.6/ 3.4/ 1.7	(0.21, 0.37) / (0.21, 0.35)	2350

	3	3.5	6.2/ 7.7/ 3.4	3.7/ 6.2/ 3.0	1.7/ 3.7/ 1.7	(0.23, 0.41) / (0.22, 0.38)	1324
	5	3.4	6.1/ 6.8/ 2.6	2.9/ 5.0/ 2.3	1.3/ 2.9/ 1.2	(0.23, 0.42) / (0.22, 0.40)	2601
	100	-	- / - / -	- / - / -	- / - / -	- / -	3
1.3	1	3.0	5.6/ 6.2/ 2.8	4.6/ 6.1/ 2.6	2.3/ 4.1/ 2.0	(0.21, 0.38) / (0.20, 0.35)	2508
	3	3.1	6.5/ 7.2/ 2.7	4.5/ 6.3/ 2.4	2.3/ 4.2/ 1.8	(0.22, 0.43) / (0.21, 0.39)	2777
	5	3.1	3.3/ 4.9/ 1.9	5.6/ 6.2/ 2.1	1.4/ 2.8/ 1.3	(0.23, 0.44) / (0.22, 0.39)	2071
	100	-	- / - / -	- / - / -	- / - / -	- / -	5

[a] Operation voltage (the voltage at 100 cd m^{-2}), [b] maximum power efficiency (PE), current efficiency (CE), and EQE of the device, [c] power efficiency (PE), current efficiency (CE), and EQE at 100 cd m^{-2}, [d] power efficiency (PE), current efficiency (CE), and EQE at 1000 cd m^{-2}, [e] CIE coordinates at 100 / 1000 cd m^{-2}.

Table S13 Measurement of the photoluminescence quantum yield (PLQY) of thin films of **1.1** doped at different concentrations into CBP host and corresponding current efficiency (CE) & external quantum efficiency (EQE) at 100 cd m^{-2} of solution-processed OLED devices.

Sample	PLQY (%)	CE_{100} (cd A^{-1})[a]	EQE_{100} (%)[b]
CBP:**1.1** (1.0 wt%)	73.11	7.9	2.9
CBP:**1.1** (3.0 wt%)	81.75	9.1	3.4
CBP:**1.1** (5.0 wt%)	66.24	4.0	1.7

[a] Current efficiency (CE) at 100 cd m^{-2}. [b] External quantum efficiency (EQE) at 100 cd m^{-2}.

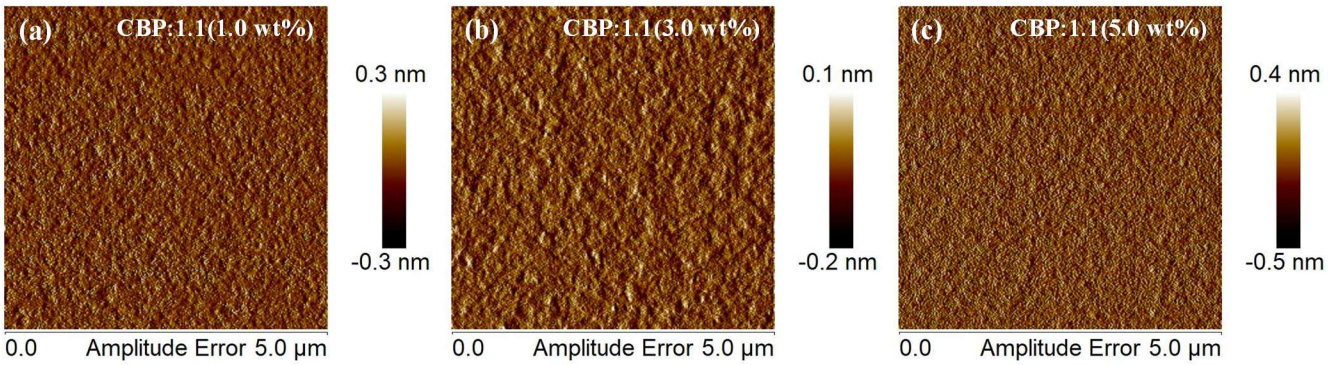

Fig. S28 AFM images of the spin-coated emitting layer films (a) CBP:**1.1** (1.0 wt%), (b) CBP:**1.1** (3.0 wt%) and (c) CBP:**1.1** (5.0 wt%).

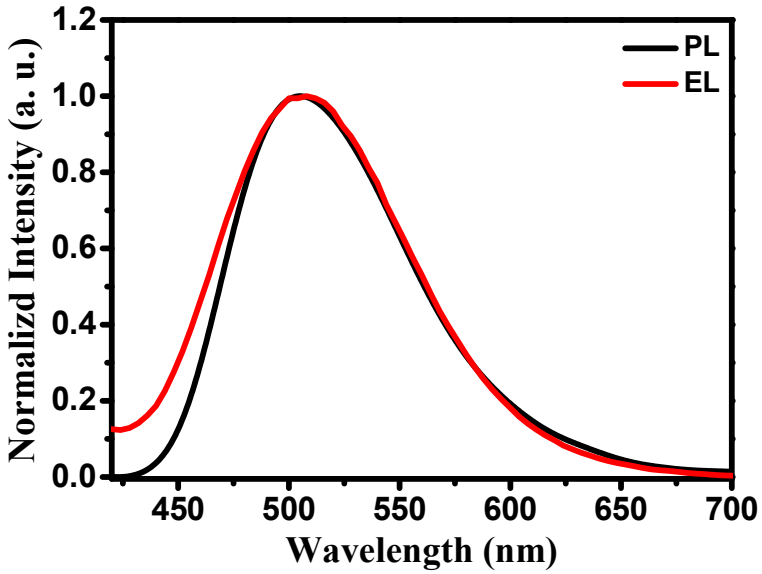

Fig. S29 PL emission spectra of compound **1.1** in solid state and EL spectra of OLED device with 3 wt% emitter (**1.1**) doped in CBP host.

References

1. J. De, S. P. Gupta, S. S. Swayamprabha, D. K. Dubey, I. Bala, I. Sarkar, G. Dey, J. H. Jou, S. Ghosh and S. K. Pal, *J. Phys. Chem. C*, 2018, **122**, 23659.
2. I. Bala, J. De, S. P. Gupta, H. Singh, U. K. Pandey and S. K. Pal, *Chem. Commun.*, 2020, **56**, 5629.
3. J. Mei, N. L. Leung, R. T. Kwok, J. W. Lam and B. Z. Tang, *Chem. Rev.*, 2015, **115**, 11718.
4. Z. Zhao, H. Zhang, J. W. Lam and B. Z. Tang, *Angew. Chem. Int. Ed.*, 2020, **59**, 9888.
5. K. Kokado and K. Sada, *Angew. Chem. Int. Ed.*, 2019, **58**, 8632.
6. Y. Hong, M. Häußler, J. W. Lam, Z. Li, K. K. Sin, Y. Dong, H. Tong, J. Liu, A. Qin, R. Renneberg and B. Z. Tang, *Chem. Eur. J.*, 2008, **14**, 6428.
7. W. Z. Yuan, P. Lu, S. Chen, J. W. Lam, Z. Wang, Y. Liu, H. S. Kwok, Y. Ma and B. Z. Tang, *Adv. Mater.*, 2010, **22**, 2159.
8. S. Jiang, J. Qiu, Y. Chen, H. Guo and F. Yang, *Dyes. Pigm.*, 2018, **159**, 533.
9. H. Jing, L. Lu, Y. Feng, J. F. Zheng, L. Deng, E. Q. Chen and X. K. Ren, *J. Phys. Chem. C*, 2016, **120**, 27577.
10. M. J. Frisch, *et* al., Gaussian 09 (Revision D.01) Gaussian, Inc., Wallingford CT, 2009**.**
11. A. D. Becke, *J. Chem. Phys.*, 1993, **98**, 5648.